

Shiga toxin glycosphingolipid receptors in microvascular and macrovascular endothelial cells: differential association with membrane lipid raft microdomains[§]

Josefine Betz,* Martina Bielaszewska,* Andrea Thies,[†] Hans-Ulrich Humpf,[†] Klaus Dreisewerd,[§] Helge Karch,* Kwang S. Kim,^{††} Alexander W. Friedrich,^{1,****} and Johannes Müthing^{1,2,****}

¹Institutes for Hygiene,* Food Chemistry,[†] Medical Physics and Biophysics,[§] and Interdisciplinary Center for Clinical Research (IZKF),** University of Münster, Münster, Germany; and Division of Pediatric Infectious Diseases,^{††} Johns Hopkins University School of Medicine, Baltimore, MD

Abstract Vascular damage caused by Shiga toxin (Stx)-producing *Escherichia coli* is largely mediated by Stxs, which in particular, injure microvascular endothelial cells in the kidneys and brain. The majority of Stxs preferentially bind to the glycosphingolipid (GSL) globotriaosylceramide (Gb3Cer) and, to a lesser extent, to globotetraosylceramide (Gb4Cer). As clustering of receptor GSLs in lipid rafts is a functional requirement for Stxs, we analyzed the distribution of Gb3Cer and Gb4Cer to membrane microdomains of human brain microvascular endothelial cells (HBMECs) and macrovascular EA.hy 926 endothelial cells by means of anti-Gb3Cer and anti-Gb4Cer antibodies. TLC immunostaining coupled with infrared matrix-assisted laser desorption/ionization (IR-MALDI) mass spectrometry revealed structural details of various lipofoms of Stx receptors and demonstrated their major distribution in detergent-resistant membranes (DRMs) compared with nonDRM fractions of HBMECs and EA.hy 926 cells. A significant preferential partitioning of different receptor lipofoms carrying C24:0/C24:1 or C16:0 fatty acid and sphingosine to DRMs was not detected in either cell type. Methyl- β -cyclodextrin (M β CD)-mediated cholesterol depletion resulted in only partial destruction of lipid rafts, accompanied by minor loss of GSLs in HBMECs. In contrast, almost entire disintegration of lipid rafts accompanied by roughly complete loss of cholesterol was detected in EA.hy 926 cells after removal of cholesterol, indicating more stable microdomains in HBMECs. Our findings provide first evidence for differently stable microdomains in human endothelial cells from different vascular beds and should serve as the basis for further exploring the functional role of lipid raft-associated Stx receptors in different cell types.—Betz, J., M. Bielaszewska, A. Thies, H-U. Humpf, K. Dreisewerd, H. Karch, K. S. Kim, A. W. Friedrich,

and J. Müthing. Shiga toxin glycosphingolipid receptors in microvascular and macrovascular endothelial cells: differential association with membrane lipid raft microdomains. *J. Lipid. Res.* 2011. 52: 618–634.

Supplementary key words glycolipid • caveolae • DRM • Gb3Cer • Gb4Cer • caveolin-1 • flotillin-2

Membrane microdomains, also named lipid rafts (1), are enriched in glycosphingolipids (GSLs) and cholesterol (2), and assembled with membrane-integrated proteins, such as caveolins or flotillins, with affinity for particular lipid species (3). Caveolins are cholesterol-binding proteins (4) and occur in flask-shaped invaginations named caveolae (5). Flotillin proteins, also called reggie proteins, are found in distinct membrane microdomains (6). Caveolae are particularly abundant in endothelial cells and are involved in many cellular processes, including cholesterol homeostasis, endocytosis, and transcytosis of macromolecules (7–9). While numerous proteomic studies have been conducted to identify lipid raft- or caveolae-associated proteins of various cell types, including endothelial cells (10–12), the GSL composition of lipid rafts or caveolae, particularly of endothelial cells, has attracted less attention, despite their outstanding role in membrane microdomain formation

Abbreviations: DRM, detergent-resistant membrane; EA.hy 926 cells, HUVEC descendant cell line; EHEC, enterohemorrhagic *Escherichia coli*; Gb3Cer, globotriaosylceramide; Gb4Cer, globotetraosylceramide; GSL, glycosphingolipid; HBMEC, human brain microvascular endothelial cell; HUVEC, human umbilical vein endothelial cell; IR-MALDI, infrared matrix-assisted laser desorption/ionization; Lc2Cer, lactosylceramide; M β CD, methyl- β -cyclodextrin; MHC, monohexosylceramide; o-TOF, orthogonal time-of-flight; Stx, Shiga toxin.

¹Senior co-author.

²To whom correspondence should be addressed.

e-mail: jm@uni-muenster.de

[§]The online version of this article (available at <http://www.jlr.org>) contains supplementary data in the form of five figures.

This work was supported by grants from the Deutsche Forschungsgemeinschaft (DFG)-funded cooperative projects MU845/4-1 (J.M.) and FR2569/1-1 (A.W.F.); the International Graduate School Molecular Interactions of Pathogens with Biotic and Abiotic Surfaces (GRK 1409, collaboration between the projects 3.10 of J.M. and 3.6 of H.K.); and the Interdisciplinary Center for Clinical Research (IZKF) Münster project no. Müth2/028/10.

Manuscript received 27 August 2010 and in revised form 18 January, 2011.

Published, JLR Papers in Press, January 20, 2011

DOI 10.1194/jlr.M010819

(13). Thus, the specific GSL composition of lipid rafts and/or caveolae of many cell types remains to be elucidated.

GSLs are built up from a hydrophobic ceramide moiety and a hydrophilic oligosaccharide residue (14, 15). They are embedded with the ceramide moiety in the outer leaflet of the plasma membrane of animal cells, where they are clustered in a more ordered state within the generally disordered milieu of the membrane. The localization of GSLs in the exofacial leaflet of the plasma membrane makes them excellent candidates as recognition structures in cell-cell interactions (16) and as receptors for numerous pathogens, such as viruses (17, 18) and bacteria (19, 20), as well as for bacterial toxins, including Shiga toxins (Stxs) (21, 22). Much effort is currently spent employing (glyco)sphingolipidomics (23–26) by use of various mass spectrometry technologies (15, 27–31) to better understanding their nature and functional role (32).

Human endothelial cells from various vascular beds compose globotriaosylceramide (Gb3Cer/CD77) and globotetraosylceramide (Gb4Cer) as major neutral GSLs, known as high- and low-affinity receptors, respectively, for Stx1 and Stx2. These GSLs have been detected in various types of endothelial cells (22), and their structures have been characterized in detail; e.g., human umbilical vein endothelial cells (HUVECs) (33–35). Vascular damage is largely mediated by Stx, which particularly injure microvascular endothelial cells in the kidney and brain (36–38). Stx are released by enterohemorrhagic *Escherichia coli* (EHEC) in the gut, translocated across the intestinal epithelium into circulation (39), and then transported to endothelial cells (39–41). The pentameric B-subunit of Stx binds to the cell surface, followed by internalization and retrograde transport via the Golgi apparatus to the endoplasmic reticulum (42). After translocation into the cytosol, the enzymatically active A-subunit exerts its toxic function through inhibition of protein biosynthesis (43, 44).

Several studies demonstrated the clustering of Gb3Cer in lipid rafts (45), the density-dependent binding of Stx with raft-localized receptors (46), and, moreover, raft-association of Stx receptors as a requirement for the retrograde transport (47, 48) and retro-translocation across the endoplasmic reticulum (49). Thus, according to present knowledge, only GSLs that associate strongly with lipid rafts can sort AB₅ toxins (including Stx) backward from the plasma membrane to the endoplasmic reticulum (50, 51). Lipid raft association of GSLs has been described so far in different cell types, such as intestinal (45, 50), HeLa, and Vero cells (47–49, 46), whereas the membrane localization of GSLs of human endothelial cells has so far not been analyzed in detail and remains largely unknown. To this day, the structural characterization of the different lipofoms of Stx GSL receptors of the macrovascular HUVEC-derived EA.hy 926 cell line and human brain microvascular endothelial cells (HBMECs) has been reported by us (52), indicating that HBMECs express both Gb3Cer and Gb4Cer, whereas EA.hy 926 cells were found to synthesize Gb3Cer but not elongated Gb4Cer.

In this study, we performed for the first time a compositional analysis of microdomains obtained as detergent-resistant membranes (DRMs) with special reference to the distribution of Stx receptors in detergent-resistant and detergent-soluble membrane fractions of HBMECs and EA.hy 926 endothelial cells. We report here on remarkable differences in microdomain composition with respect to the occurrence of Stx receptors and, moreover, on differential lipid raft stability toward cholesterol-depletion of the two endothelial cell types, where raft disintegration was found to be accompanied by loss of Stx receptors in DRM fractions. The newly developed technique combining thin-layer chromatography (TLC) separation and immunodetection of Stx receptors on the TLC plate with infrared matrix-assisted laser desorption/ionization orthogonal time-of-flight mass spectrometry (IR-MALDI-o-TOF-MS) served as an indispensable tool for structural analysis of small GSL amounts directly on the TLC plate (15).

MATERIALS AND METHODS

Endothelial cells and cell cultivation

HBMECs (53) were cultured in RPMI 1640 medium (Lonza, Cologne, Germany) supplemented with 10% fetal calf serum (FCS) (PAA, Pasching, Austria), 10% Nu-Serum (Becton Dickinson Biosciences, Bedford, MA), 2 mM L-glutamine, 1 mM sodium pyruvate, 1.0 U/ml MEM nonessential amino acids, and 1.0 U/ml vitamins (Lonza). EA.hy 926 cells (54) were cultivated in DMEM:F12 (1:1) culture medium (Lonza) containing 10% FCS. Both cell lines were maintained at 37°C in a humidified atmosphere containing 5% CO₂ in air. To investigate the influence of the cell culture medium on GSL and protein expression, EA.hy 926 cells were alternatively grown in the same medium as HBMECs (= RPMI 1640 medium with supplements as outlined above).

Methyl- β -cyclodextrin treatment of endothelial cells

The influence on the cellular integrity upon methyl- β -cyclodextrin (M β CD)-mediated cholesterol depletion was controlled microscopically. For this purpose, endothelial cells were grown in 24-well tissue culture plates (Greiner Bio-One, Frickenhausen, Germany) until confluence in media as described above and treated for 1 h with cell-culture-tested M β CD (Sigma-Aldrich Chemie GmbH, Steinheim, Germany), with increasing concentrations from 1 mM to 50 mM M β CD in serum-free medium. Additional control cell culture experiments without M β CD were performed for 1 h with serum-supplemented medium (see previous section), under serum-free conditions and with phosphate-buffered saline (PBS). Cells were evaluated at 20 \times and 100 \times magnification using an Axiovert 40 inverse microscope (Zeiss, Göttingen, Germany) fitted with an AxioVision 3.1 digital camera (Zeiss, 1,360 \times 1,040 pixel). Data were processed with Adobe Photoshop software (Adobe Systems Inc., San Jose, CA).

For lipid and protein analysis, endothelial cells were grown each in two 175 cm² tissue culture flasks until 80% confluence in serum-supplemented medium (see above), washed twice with prewarmed serum-free medium, and incubated for 1 h in serum-free medium with 10 mM M β CD. The ensuing lipid and protein extraction was performed as described below.

Lipid extraction and isolation of neutral GSLs from endothelial cells

Confluent grown cells from four 175 cm² tissue culture flasks (Greiner) were trypsinized and washed with prewarmed PBS.

GSLs were sequentially extracted from the sediments with 15 ml each of methanol, chloroform/methanol (1/2, v/v), chloroform/methanol (1/1, v/v), and chloroform/methanol (2/1, v/v). The combined supernatants were dried by rotary evaporation, and phospholipids were saponified by incubation in 20 ml of aqueous 1N NaOH for 1 h at 37°C. After neutralization with 2 ml of 10 N HCl, the samples were dialyzed against deionized water and dried by rotary evaporation. Neutral GSLs were separated from gangliosides by anion-exchange column chromatography employing DEAE-Sepharose CL-6B (GE Healthcare, Munich, Germany) in the acetate form and purified by silica gel 60 (particle size 0.040-0.063 mm, Merck, Darmstadt, Germany) chromatography according to standard procedures (55, 56). The neutral GSL fractions were adjusted to defined volumes of chloroform/methanol (2/1, v/v) corresponding to 1×10^5 cells per μl .

Antibodies

The specificities of polyclonal chicken IgY anti-Gb3Cer and anti-Gb4Cer antibodies have been reported in previous publications (57–60). Rat IgM monoclonal anti-Gb3Cer/CD77 antibody 38.13 (Catalog No. IM0175) was obtained from Beckman Coulter (Krefeld, Germany). Rabbit polyclonal anti-caveolin-1 antibody (Catalog No. 3238) and rabbit IgG monoclonal anti-flotillin-2 C42A3 (Catalog No. 3436) were purchased from Cell Signaling Technology (Danvers, MA) and mouse IgG monoclonal anti-flotillin-2 B-6 antibody (Catalog No. sc-28320) was from Santa Cruz Biotechnology, Inc. (Heidelberg, Germany).

Secondary alkaline phosphatase-conjugated polyclonal rabbit anti-chicken IgY (Code 303-055-033) and goat anti-rabbit IgG (Code 111-055-003) antibodies were from Jackson ImmunoResearch (West Grove, PA). Alexa Fluor[®] 546 goat anti-rat IgG+IgM, Alexa Fluor[®] 488 goat anti-mouse IgG, and Cy5[®] goat anti-rabbit IgG were obtained from Invitrogen/Molecular Probes (Karlsruhe, Germany).

Reference GSLs and proteins

A mixture of neutral GSLs from human erythrocytes, consisting of monohexosylceramide (MHC), lactosylceramide (Lc2Cer or Gal β 4Glc β 1Cer), globotriaosylceramide (Gb3Cer or Gal α 4Gal β 4Glc β 1Cer), and globotetraosylceramide (Gb4Cer or GalNAc β 3Gal α 4Gal β 4Glc β 1Cer), was used as reference (57). The nomenclature of the GSLs follows the IUPAC-IUB recommendations 1997 (61).

Human heart whole-cell lysate containing caveolin proteins (Catalog No. ab29431, Abcam, Cambridge, MA) and HeLa whole-cell lysate containing flotillin proteins (Catalog No. sc-2200, Santa Cruz Biotechnology) were used as positive controls.

Immunofluorescence microscopy

HBMECs and EA.hy 926 cells were seeded in 8-well polystyrene chamber slides (tissue culture chambers, Permax[™], Nunc GmbH) in amounts of 1.5×10^4 and 3×10^4 cells/chamber, respectively, and grown for 24 h until ~80% confluence. Medium was aspirated, and cells were washed with prewarmed PBS (Lonza) and fixed for 30 min at room temperature with 3.7% paraformaldehyde (Merck). If not otherwise stated, the following steps were performed at ambient temperature. The fixed cells were washed with PBS and quenched for 15 min with 0.2 M glycine (Roth, Karlsruhe, Germany; pH 7.2). After twofold washing with PBS, cells were blocked and permeabilized with 5% (w/v) BSA (Serva Electrophoresis, Heidelberg, Germany), 0.2% (v/v) fish skin gelatin (Sigma-Aldrich) and 0.3% Triton (v/v) X-100 (Serva Electrophoresis) in PBS for 2 h. After washing with PBS, the slides were incubated overnight at 4°C with anti-Gb3Cer antibody 38.13, anti-caveolin-1, or anti-flotillin-2 antibody, each di-

luted 1:500 in PBS with 1% BSA and 0.3% Triton X-100. The slides were then washed three times with PBS and incubated for 1 h under light protection with fluorochrome-labeled secondary antibodies diluted 1:1000 in PBS with 1% BSA and 0.3% Triton X-100. After threefold washing in PBS, nuclear DNA was stained for 10 min with 4',6-diamidino-2-phenylindol (DAPI, Sigma-Aldrich) in PBS (20 ng/ml), and the slides were embedded in antifading mounting medium (Dianova, Hamburg, Germany). Controls without primary antibodies were processed in parallel. Bound fluorochrome-labeled antibodies and stained nuclei were visualized under a fluorescence microscope (Axio Imager.A1, Zeiss), original magnification $\times 100$, with filter sets adequate to the maxima of absorption/emission of Cy5[®] (649 nm/670 nm), Alexa Fluor[®] 488 (495 nm/519 nm), Alexa Fluor[®] 546 (556 nm/573 nm), and DAPI (368 nm/488 nm). The fluorescence was recorded with an AxioCam CCD camera (Zeiss), documented with AxioVision 4.8, and processed with Adobe Photoshop software (Adobe Systems Inc.).

High-performance TLC and TLC immunostaining

Application of purified GSLs, lipid extracts, and cholesterol solutions to silica gel 60 pre-coated glass plates (HPTLC plates, size 10 cm \times 10 cm, thickness 0.2 mm, No. 1.05633.0001; Merck) was accomplished with an automatic sample applicator (Linomat IV, CAMAG, Muttenz, Switzerland). Neutral GSLs were separated in the solvent chloroform/methanol/water (120/170/17, each by vol.) in a saturated chamber for 20 min and stained with orcinol (62). Cholesterol was determined after TLC separation for 20 min in the solvent chloroform/acetone (96/4, v/v) after dipping the plate for 2 s in a mangan(II)chloride sulfuric acid solution (0.2 g mangan(II)chloride-tetrahydrate (Mn(II)Cl $_2$ \times 4 H $_2$ O) in 60 ml of methanol/water (1/1, v/v) acidified with 2 ml of concentrated H $_2$ SO $_4$) and heating for 15 min at 120°C on a TLC Plate Heater III (CAMAG) (63). Dark brown cholesterol bands were quantified in triplicate with a CD60 scanner (Desaga, Heidelberg, Germany, software ProQuant[®], version 1.06.000) in reflectance mode at a wavelength of $\lambda = 365$ nm with a light beam split of 0.02 mm \times 3 mm. A cholesterol (Riedel-de Haen, Seelze, Germany) solution of 0.1 $\mu\text{g}/\mu\text{l}$ chloroform/methanol (2/1, v/v) was used as reference.

The TLC immunodetection procedure using polyclonal chicken anti-Gb3Cer and anti-Gb4Cer antibodies (1:2000 dilution) was employed as previously described (57, 59, 62, 64). Alkaline phosphatase-labeled secondary antibodies were used in 1:2000 dilutions. All dilutions were performed in 1% (w/v) BSA in PBS and bound secondary antibodies were visualized by color development using 0.05% (w/v) 5-bromo-4-chloro-3-indolyl phosphate *p*-toluidine salt (BCIP; Roth) in glycine buffer (pH 10.4).

Preparation of DRMs

The preparation of DRMs was done according to Brown and Rose (65) with minor modifications. Detergent extractions were done on ice with prechilled solutions. Membranes from confluent grown cells were disintegrated by cell lysis in 10 mM HEPES pH 7.4, 42 mM KCl, 5 mM MgCl $_2$, and protease-/phosphatase-inhibitors (Complete, Mini cocktail tablets, Roche Diagnostics) under sonication (Sonifier Bandelin Sonopuls HD 2070, 20 counts, each 2 s, 80% power). Cell debris was removed by centrifugation at 400 *g* for 10 min at 4°C, followed by ultracentrifugation of the supernatant at 150,000 *g* for 30 min at 4°C to separate cytosol from remaining membranes. The membrane sediment was resuspended with a 20G \times 11/2 drain tube 0.9 mm \times 40 mm (Microlance[™] 3, BD, Heidelberg, Germany) in 1 ml of 1% Triton X-100 (v/v) in TNE-buffer (10 mM Tris pH 7.5, 150 mM NaCl, 5 mM EDTA) and kept on ice for 30 min. The resuspension procedure was repeated twice with 30 min breaks between

the steps. The homogenous solution was then overlaid with a discontinuous sucrose bottom-to-top gradient of 42.5%, 30%, and 5% sucrose (each w/v) in TNE-buffer. DRMs were separated from the bulk of detergent-soluble membrane lipids by ultracentrifugation at 200,000 *g* for 19 h at 4°C owing to their lower buoyant density whereby the light DRMs float to the interface between 5% and 30% sucrose in the density gradient. Eight fractions of 1.5 ml volume each were collected from top to bottom and the sediment was dissolved in 1.5 ml of PBS (= fraction 9). A scheme of the procedure is provided as supplementary Fig. 1.

Isolation of GSLs, cholesterol, and proteins from density gradient fractions

Lipids, including GSLs and cholesterol, were extracted from 1.2 ml of each fraction. Phospholipids were saponified by adding 120 μ l 10 M NaOH under gentle agitation for 1 h at 37°C. After neutralization with 120 μ l of 10 M HCl, the samples were dialyzed at 4°C for two days against deionized water and dried by rotary evaporation. The extracts were dissolved under short sonication in chloroform/methanol (2/1, v/v) and adjusted to defined volumes of chloroform/methanol (2/1, v/v) corresponding to 1×10^4 cells per μ l. GSLs and cholesterol were analyzed by TLC as described above.

Volumes of 0.3 ml of each density gradient fraction (see above) were dialyzed for two days at 4°C against deionized water to remove sucrose. Protein concentrations were determined in triplicate in maxi-sorp 96-well microtiter plates (Nunc) according to Lowry et al. (66) at an absorbance wavelength of $\lambda = 630$ nm using an EL800 microwell plate reader (BioTek Instruments, Bad Friedrichshall, Germany; software Gen5™) and BSA as reference protein. Proteins were precipitated with 5% (w/v) trichloroacetic acid, washed with absolute ethanol, and applied to SDS-PAGE. Three independent experiments were performed, and representative measurements are shown in the results section.

SDS-PAGE and Western blotting

The precipitated proteins of the density gradient fractions were dissolved in $1 \times$ sample buffer, heated for 5 min at 95°C, and loaded onto the gels. SDS-PAGE separation was done under reducing conditions using 4% stacking and 12% separating gels of 0.75 mm thickness (67). Standard proteins in a molecular range from 14 kDa to 66 kDa were used as references (Dalton Mark VII-L; Sigma-Aldrich). Proteins were fixed with 20% methanol in 25 mM Tris buffer (pH 8.25) supplemented with 192 mM glycine. SDS-PAGE-separated proteins were transferred by means of a semi-dry blotting system onto a nitrocellulose membrane (Amersham Hybond™-C Extra; GE Healthcare, Freiburg, Germany). Nonspecific binding was blocked by incubating the membrane for 1 h in Tris-buffered saline with 0.1% (v/v) Tween-20 (TBS/T) supplemented with 3% (w/v) BSA (= blocking solution, pH 7.6). After washing with TBS/T, the membrane was overlaid with anti-caveolin-1 or anti-flotillin-2 antibodies (diluted 1:4000 in blocking solution) with gentle agitation overnight at 4°C. The membrane was then washed three times for 5 min each with TBS/T, followed by incubation with alkaline phosphatase-labeled anti-rabbit IgG secondary antibody (diluted 1:2000 in blocking solution) for 1 h. After three washings with TBS/T, bound antibodies were visualized with 0.005% (w/v) BCIP and 0.01% (w/v) nitroblue tetrazolium (NBT/BCIP kit; Invitrogen).

IR-MALDI-o-TOF-MS

The specifications of the orthogonal time-of-flight mass spectrometer (MDS Sciex, Concord, ON, Canada) have been outlined in detail in previous studies (64, 68). Direct TLC-IR-MALDI-o-TOF-MS analysis was performed in situ from immunopositive GSL bands utilizing a Q-switched Er:YAG laser (Speser, $\lambda = 2.94$

μ m, $\tau \sim 100$ ns; Spektrum, Berlin). The focal laser spot size was about $200 \mu\text{m} \times 300 \mu\text{m}$. After soaking of the BCIP-stained TLC stripes for 2 h in 10 mM ammonium acetate buffer (pH 3.6) and drying at room temperature, Plexigum P28 was removed by threefold consecutive dipping in distilled chloroform. For MS analysis, the TLC stripes were cut to pieces of $\sim 15 \text{ mm} \times 40 \text{ mm}$ to fit into the custom-made MALDI sample plate. A matrix of 0.3 μ l drops of glycerol was applied with a pipet across the positive GSL bands. Spectra were acquired in the positive ion mode. About 300 laser shots at a fixed laser fluence were applied to the GSL bands to obtain a measure for relative variation of GSL abundances. Absolute quantities cannot be derived from the IR-MALDI-MS spectra.

RESULTS

Detection of Stx receptors in neutral GSL fractions of total cells using TLC overlay assay

GSLs were extracted from both HBMECs and EA.hy 926 cells. Neutral GSLs were isolated by anion-exchange chromatography. Aliquots of neutral GSLs equivalent to identical cell quantities were separated by TLC followed by orcinol staining and immunodetection (Fig. 1). Stx receptors of the globo-series were immunostained with anti-Gb3Cer antibody (Fig. 1A) and anti-Gb4Cer antibody (Fig. 1B) in addition to orcinol staining (Fig. 1C). The anti-Gb3Cer antibody bound to Gb3Cer of HBMECs and EA.hy 926 cells (Fig. 1A, lane b and c, respectively) where upper bands harbor Gb3Cer structures with mostly C24 and lower bands Gb3Cer with C16 fatty acid, which were verified by IR-MALDI-o-TOF-MS (see next section). The anti-Gb4Cer assay demonstrated that Gb4Cer is present in HBMECs (Fig. 1B, lane b), but undetectable in EA.hy 926 cells (Fig. 1B, lane c), which is in agreement with the results of the orcinol stain (Fig. 1C) and previous investigations (52).

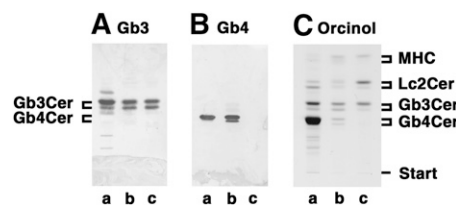


Fig. 1. Antibody-mediated detection of globo-series neutral GSLs in HBMECs and EA.hy 926 cells. GSL quantities used in the anti-Gb3Cer (A) and the anti-Gb4Cer (B) TLC immunostains are equivalent to 2×10^5 cells and 2 μ g (A) and 0.2 μ g (B) of neutral GSLs from human erythrocytes, and those for the orcinol stain (C) correspond to 1×10^6 cells and 20 μ g of neutral GSLs from human erythrocytes. Bound anti-GSL antibodies were visualized with alkaline phosphatase conjugated secondary antibodies and BCIP as a substrate. Lanes a: human erythrocytes; lanes b: HBMECs; lanes c: EA.hy 926 cells. Panel headings Gb3 and Gb4 stand for anti-Gb3Cer and anti-Gb4Cer overlay staining, respectively. EA.hy 926 cells, HUVEC descendant cell line; Gb3Cer, globotriaosylceramide; Gb4Cer, globotetraosylceramide; GSL, glycosphingolipid; HBMEC, human brain microvascular endothelial cell; MHC, monohexosylceramide.

IR-MALDI-o-TOF-MS of Stx receptors in the neutral GSL fractions of total cells

The immunodetected Gb3Cer bands of total HBMECs and EA.hy 926 cells were analyzed by in situ IR-MALDI-o-TOF-MS directly on the TLC plate as shown in Fig. 2. Gb3Cer species appear as monosodiated $[M+Na]^+$ ions in the positive ion mode mass spectra. The major ions of the anti-Gb3Cer positive upper band of HBMECs at m/z 1158.78 indicate predominance of Gb3Cer (d18:1, C24:0), accompanied by low abundant ions at m/z 1156.77 and 1130.76 indicative of Gb3Cer (d18:1, C24:1) and Gb3Cer (d18:1, C22:0), respectively (Fig. 2A, left panel). The high abundant $[M+Na]^+$ ions acquired from the lower Gb3Cer band at m/z 1046.68 confirmed the presence of Gb3Cer (d18:1, C16:0) (Fig. 2A, right panel). The same Gb3Cer variants could be deduced from the mass spectra that were obtained from immunoreactive Gb3Cer upper and lower bands of EA.hy 926 cells (Fig. 2B, left and right panels).

In addition, traces of ions in the spectrum at m/z 1186.80 gave evidence for the presence of Gb3Cer (d18:1, C26:0) in EA.hy 926 cells not found in the upper band spectrum of HBMECs. A synopsis of the relative m/z intensities attributable to the different Gb3Cer lipofoms is presented in Table 1.

Direct ionization of immunodetected GSLs on chromatograms allows in situ structural characterization by IR-MALDI-o-TOF-MS, omitting scratching of the silica gel from the plate and ensuing extraction of GSLs. Moreover, GSLs can be comparatively analyzed without any loss of analyte of particular interest in case of small GSL amounts, e.g., isolated from DRM fractions (see below). These are the major advantages of this approach compared with previous investigations, where the Stx receptors of HBMECs and EA.hy 926 cells were analyzed from pooled silica gel extracts of several TLC runs (52).

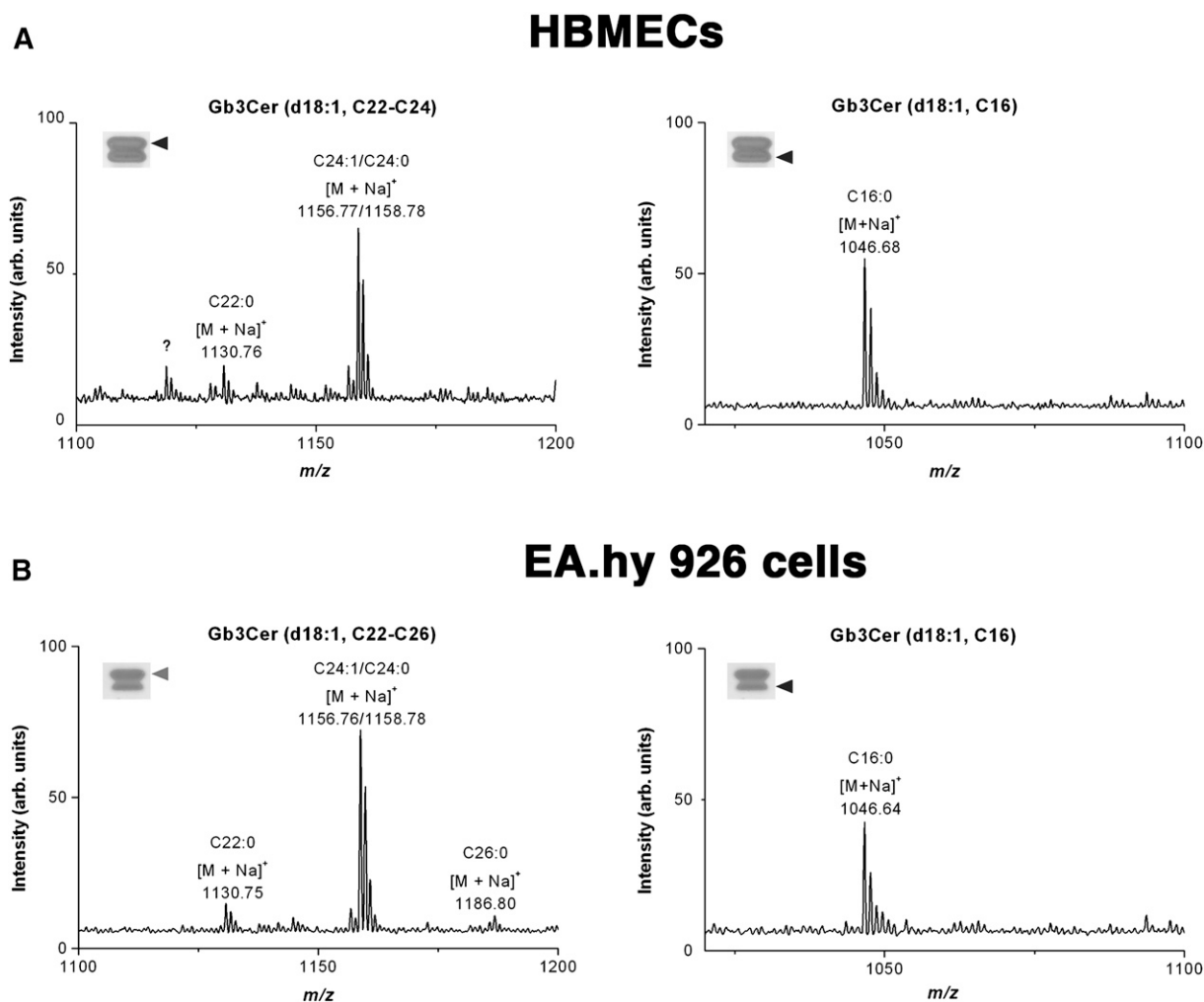


Fig. 2. TLC-IR-MALDI-o-TOF mass spectra obtained from antibody-detected Gb3Cer species of HBMECs (A) and EA.hy 926 cells (B). The overlay assays were performed with TLC-separated neutral GSLs corresponding to 3×10^5 cells as described in Fig. 1. The in situ analyzed Gb3Cer positive upper bands (left panels) and lower bands (right panels) are marked with arrowheads in the insets. Mass spectra were acquired in the positive ion mode; Gb3Cer species were detected as singly charged monosodiated $[M+Na]^+$ ions. Relative ion intensities of detected Gb3Cer variants are listed in Table 1. EA.hy 926 cells, HUVEC descendant cell line; Gb3Cer, globotriaosylceramide; Gb4Cer, globotetraosylceramide; GSL, glycosphingolipid; HBMEC, human brain microvascular endothelial cell; IR-MALDI, infrared matrix-assisted laser desorption/ionization; o-TOF, orthogonal time-of-flight.

TABLE 1. Relative ion intensities from immunostained anti-Gb3Cer bands of total endothelial cells and DRM F2

Gb3Cer Lipoforms	Total Cells	DRM F2
HBMECs		
Gb3Cer (d18:1, C24:0)	+++	+++
Gb3Cer (d18:1, C24:1)	+	++
Gb3Cer (d18:1, C22:0)	+	+
Gb3Cer (d18:1, C16:0)	+++	+++
EA.hy 926 cells		
Gb3Cer (d18:1, C26:0)	(+)	+
Gb3Cer (d18:1, C24:0)	+++	+++
Gb3Cer (d18:1, C24:1)	(+)	-
Gb3Cer (d18:1, C22:0)	+	-
Gb3Cer (d18:1, C16:0)	+++	+++

Relative ion intensities were determined by in situ TLC-IR-MALDI-o-TOF-MS in positive ion mode. Neutral GSLs from total endothelial cells were purified by anion-exchange column chromatography. DRM fraction 2 (F2) was obtained by sucrose density gradient centrifugation (see supplementary Fig. 1). GSL-containing extracts were prepared from DRM F2 by chloroform/methanol extraction. Relative [M+Na]⁺ ion intensities: -, not detectable; (+), traces; +, low; ++, moderate; +++, high. Ion intensities were estimated from upper and lower immunopositive bands from total cells (Fig. 2) and DRM F2 (Fig. 6) containing Gb3Cer species with long-chain (C22-C26) and short-chain (C16) fatty acids, respectively. DRM, detergent-resistant membrane; EA.hy 926 cells, HUVEC descendant cell line; F2, fraction 2; Gb3Cer, globotriaosylceramide; GSL, glycosphingolipid; HBMEC, human brain microvascular endothelial cell; IR-MALDI, infrared matrix-assisted laser desorption/ionization; o-TOF, orthogonal time-of-flight.

Cholesterol and protein content of sucrose density gradient fractions

Lipids were extracted from 1.2 ml and proteins were prepared from 0.3 ml aliquots of the nine fractions (1.5 ml each), which were obtained from HBMEC and EA.hy 926 cell homogenates by sucrose density gradient centrifugation using 1% Triton X-100 (supplementary Fig. 1). The cholesterol and protein contents were calculated as micrograms per 1×10^6 cells. The distribution of cholesterol and protein to the gradient fractions of both cell lines is shown in Fig. 3. The highest quantities of cholesterol were determined in the DRM fraction 2 and adjacent fractions 1 and 3 as expected (Fig. 3A). The intermediate fractions 4 to 7 and the bottom fraction 8 are characterized by very low cholesterol concentrations, whereas the sediment fraction 9 exhibited a slight enrichment compared with the nonDRM fractions. Notably, cell cholesterol contents of the DRM fraction 2 and contiguous fraction 3 from EA.hy 926 cells were 1.8-fold and 1.4-fold higher, respectively, and equal in fraction 1 compared with HBMECs (Fig. 3A). Compared with cholesterol, the protein distribution was inverted in the gradient fractions. Proteins increased in nonDRM fraction 7, and the bulk of proteins accumulated in the bottom fraction 8 and the sediment fraction 9 (Fig. 3B), whereas DRM fraction 2 and flanking fraction 3 harbored only minor quantities of proteins and were almost indistinguishable from the intermediate fractions 4 to 6 with regard to the protein content. These gradient profiles demonstrate predominant distribution of microdomain-associated cholesterol to DRM fractions and preferential occurrence of soluble membrane proteins in nonDRM fractions in both endo-

thelial cell lines. Interestingly, the cholesterol content was found in average 1.4-fold higher in EA.hy 926 cells (calculated for DRM fractions 1 to 3).

Distribution of Gb3Cer and Gb4Cer to sucrose gradient fractions of HBMECs

The lipid extracts and protein preparations of the sucrose density gradient fractions of HBMECs were subjected to TLC immunodetection of Gb3Cer and Gb4Cer and Western blot analysis of caveolin-1 and flotillin-2 (Fig. 4). DRM fraction 2 exhibited the highest relative quantity of Gb3Cer (54%), followed by fractions 1 and 3 with 21% and 14%, respectively (Fig. 4A, upper panel). Thus, 89% of Gb3Cer floated in the DRM fractions; the residual 7% were made up of soluble Gb3Cer, which distributed more or less equally to the nonDRM fractions 4 to 8, and 4% were found in the sediment fraction. The determination of the relative quantities of Gb3Cer with long- (upper band) to short-chain (lower band) fatty acids [i.e., of

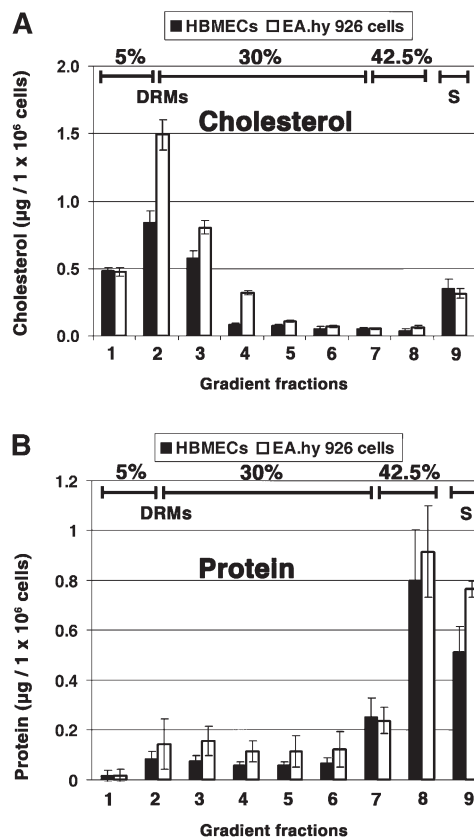


Fig. 3. Cholesterol (A) and protein (B) content in sucrose density gradient fractions of HBMECs (black bars) and EA.hy 926 cells (white bars). Gradient fractions were numbered from top (= fraction 1) to bottom (= fraction 8); fraction 9 was obtained by solubilization of the sediment (see supplementary Fig. 1). Lipid extracts were separated by TLC, and cholesterol was quantified by densitometric scanning. Stained proteins were quantified colorimetrically by extinction measurement in microtiter plates. Results represent the means and standard deviations of 3-fold determination and are expressed as micrograms per 1×10^6 cells. DRM, detergent-resistant membrane; EA.hy 926 cells, HUVEC descendant cell line; HBMEC, human brain microvascular endothelial cell; S, sediment fraction.

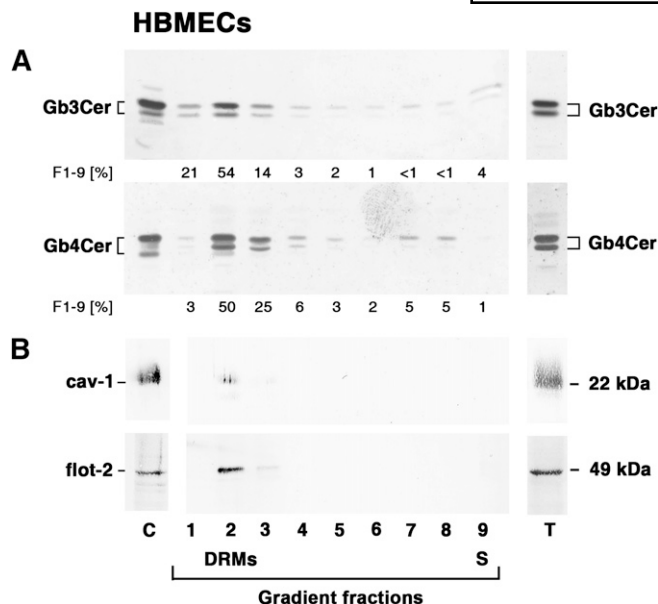


Fig. 4. Detection of Gb3Cer and Gb4Cer (A) and caveolin-1 and flotillin-2 (B) in sucrose gradient fractions of HBMECs. Gradient fractions were numbered from top (= fraction 1) to bottom (= fraction 8); fraction 9 was obtained by solubilization of the sediment (see supplementary Fig. 1). A: TLC overlay assays. Lipid extracts were separated by TLC, and Gb3Cer and Gb4Cer were immunodetected with anti-Gb3Cer (upper panel) and anti-Gb4Cer antibody (lower panel). Control (C): 2 μ g and 0.2 μ g of neutral GSLs from human erythrocytes for anti-Gb3Cer and anti-Gb4Cer immunostain, respectively; GSL amounts of the gradient fractions 1 to 9 (F1-9) correspond to 5×10^5 cells and those of total cells (T) are equivalent to 2.5×10^5 cells. The relative amounts of Gb3Cer and Gb4Cer in the gradient fractions (F1-9) were determined densitometrically and are given as percentages in the figure; different Gb3Cer and Gb4Cer lipofoms (upper and lower bands) of total cells and DRM fraction 2 are listed as percentages in Table 2. B: Western blots. Protein preparations were separated by SDS-PAGE and transferred onto nitrocellulose membranes. Caveolin-1 and flotillin-2 were detected with anti-caveolin-1 (upper panel) and anti-flotillin-2 antibody (lower panel). Control (C): 10 μ g of human heart lysate and 20 μ g of HeLa cell lysate for caveolin-1 and flotillin-2 immunodetection, respectively; protein amounts of the sucrose gradient fractions 1-9 and total cells (T) correspond to 1×10^6 cells, respectively. Vertical white lines indicate areas of non-contiguous lanes assembled. DRM, detergent-resistant membrane; Gb3Cer, globotriaosylceramide; Gb4Cer, globotetraosylceramide; GSL, glycosphingolipid; HBMEC, human brain microvascular endothelial cell; S, sediment fraction.

Gb3Cer (d18:1, C22-C24) to Gb3Cer (d18:1, C16)] revealed 65% and 59% of Gb3Cer (d18:1, C22-C24) in DRM fraction 2 and total cells, respectively, indicating a minor enhancement of Gb3Cer species with long-chain fatty acids in DRM fraction 2 (Table 2). This result was previously obtained by Falguières et al. in HeLa cells (48).

A similar gradient distribution pattern was observed for Gb4Cer with predominant occurrence in DRM fraction 2 (50%) followed by fractions 3 and 1 with 25% and 3%, respectively (Fig. 4A, lower panel). Thus, 78% of Gb4Cer floated in the DRM fractions. The residual 21% constituted soluble Gb4Cer in the nonDRM fractions 4 to 8, and only 1% was detectable in the sediment fraction. The relative distribution of upper band Gb4Cer (d18:1, C22-C24)

compared with lower band Gb4Cer (d18:1, C16:0) was virtually identical in DRM fraction 2 and total cells, where Gb4Cer (d18:1, C22-C24) amounted to 57% and 59%, respectively (Table 2). In conclusion, these data suggest that both Gb3Cer and Gb4Cer reside preferentially, but not exclusively, in the DRM fractions. The calculated mean values of Gb3Cer and Gb4Cer residing in DRM fractions from three individual experiments gave 83% (SD \pm 5.0) and 54% (SD \pm 15.1), respectively, indicating that DRM association was more pronounced for Gb3Cer, corresponding to a remarkably higher ratio of soluble Gb4Cer in the nonDRM fractions. Moreover, a subtle enrichment of Gb3Cer with long-chain fatty acids was detectable in the major DRM fraction 2 of HBMECs.

Western blot analysis of the dissemination of the caveolae marker protein caveolin-1 revealed low but exclusive occurrence of caveolin-1 in DRM fraction 2 (Fig. 4B, upper panel). Interestingly, the higher level of caveolin-1 in the protein preparation of total cells indicated that only a minor quantity of caveolin-1 resided in membrane microdomains of DRM fraction 2. The lipid raft marker protein flotillin-2 was found to preferentially partitioned, like caveolin-1, to DRM fraction 2, but on an apparently higher level than caveolin-1 compared to flotillin-2 in total cells (Fig. 4B, lower panel). In summary, the distribution pattern of Gb3Cer and Gb4Cer TLC overlay assays and the Western blots of caveolin-1 and flotillin-2 clearly evidenced colocalization of both GSLs with lipid raft marker proteins in DRM fractions. Furthermore, the data suggested a preferential occurrence of lipid rafts harboring flotillin-2 and only minor existence of caveolin-1-containing caveolae in DRM fractions of HBMECs.

Distribution of Gb3Cer to sucrose gradient fractions of EA.hy 926 cells

TLC immunodetection of Gb3Cer in lipid extracts and Western blots of caveolin-1 and flotillin-2 in protein preparations of the gradient fractions obtained from EA.hy 926 cells were performed as with HBMECs (Fig. 5). Gb3Cer was found preferentially in DRM fraction 2 and adjacent fraction 3 amounting to 28% and 15%, respectively, accompanied by only 3% in fraction 1 (Fig. 5A). Thus, 46% of Gb3Cer floated in the DRM fractions. The remaining 32% were made up of soluble Gb3Cer, which distributed almost equally to the nonDRM fractions 4 to 8, and 22% were detected in the sediment fraction. The relative quantities of Gb3Cer (d18:1, C22-C26) to Gb3Cer (d18:1, C16) were almost identical in DRM fraction 2 and total cells where Gb3Cer (d18:1, C22-C26) constituted 70% and 67%, respectively, indicating a minor relative increase of Gb3Cer with long-chain fatty acids in DRM fraction 2 (Table 2). In conclusion, Gb3Cer was found to reside preferentially, but not exclusively, in the DRM fractions. Importantly, EA.hy 926 cells exhibited only half of the flotation rate of Gb3Cer in DRM fractions and 3-fold higher amounts of soluble Gb3Cer in the nonDRM fractions compared to HBMECs.

Western blot analysis of caveolin-1 showed strong and moderate appearances of caveolin-1 in DRM fraction 2

TABLE 2. Relative distribution of Gb3Cer and Gb4Cer lipofoms with long- and short-chain fatty acids in total endothelial cells and DRM F2 without and after M β CD treatment

Gb3Cer and Gb4Cer Lipofoms	Total Cells	DRM F2	10 mM M β CD	
			Total Cells	DRM F2
	%	%	%	%
HBMECs				
Gb3Cer (d18:1, C22-C24)	59	65	58	67
Gb3Cer (d18:1, C16)	41	35	42	33
Gb4Cer (d18:1, C22-C24)	59	57	62	73
Gb4Cer (d18:1, C16)	41	43	38	27
EA.hy 926 cells				
Gb3Cer (d18:1, C22-C26)	67	70	66	67
Gb3Cer (d18:1, C16)	33	30	34	33

Relative distribution of Gb3Cer and Gb4Cer lipofoms with long-chain (C22-C26, upper bands) and short-chain (C16, lower bands) fatty acids in double bands was determined by TLC scanning densitometry using GSL extracts of total endothelial cells and DRM F2 (see supplementary Fig. I) without (see Figs. 4 and 5) and after 10 mM M β CD treatment (see Figs. 9 and 10). DRM, detergent-resistant membrane; EA.hy 926 cells, HUVEC descendant cell line; Gb3Cer, globotriaosylceramide; Gb4Cer, globotetraosylceramide; GSL, glycosphingolipid; HBMEC, human brain microvascular endothelial cell; M β CD, methyl- β -cyclodextrin.

and adjacent fraction 3, respectively (Fig. 5B, upper panel). Compared with the protein preparation of total cells, it was obvious that high amounts of caveolin-1 localized to membrane microdomains. Notably, flotillin-2 was undetectable in DRM fraction 2 and in accompanying gradient fractions and appeared only in traces in the bottom fraction 8 (Fig. 5B, lower panel). In summary, our results unequivocally evidenced colocalization of Gb3Cer with the caveolae marker protein caveolin-1 in DRM fractions and suggested the absence of flotillin-2-harboring lipid rafts in EA.hy 926 cells.

IR-MALDI-o-TOF-MS of Stx receptors in DRM fraction 2

The immunodetected Gb3Cer species of DRM fraction 2 of HBMECs (Fig. 4A) and of EA.hy 926 cells (Fig. 5A) were further structurally characterized by in situ IR-MALDI-o-TOF-MS (Fig. 6). The predominance of Gb3Cer (d18:1, C24:1/C24:0) in the upper Gb3Cer immunopositive band of HBMECs is evidenced by monosodiated $[M+Na]^+$ ions at m/z 1156.79/1158.81 (Fig. 6A, left panel) flanked by minor ions at m/z 1130.78 corresponding to Gb3Cer (d18:1, C22:0). Importantly, the enhanced signal intensity of ions at m/z 1156.79 compared with those at m/z 1158.81 indicated a relative increase of Gb3Cer (d18:1, C24:1) in the DRM fraction 2 of HBMECs compared with the mass spectrum acquired from the upper Gb3Cer band of the neutral GSL fraction of total HBMECs (Fig. 2A, left panel). The lower Gb3Cer positive band of DRM fraction 2 harbored Gb3Cer (d18:1, C16:0), indicated by high abundant $[M+Na]^+$ ions at m/z 1046.72 (Fig. 6A, right panel).

Interestingly, in the DRM fraction 2 of EA.hy 926 cells, the dominant monosodiated ions at m/z 1158.80 related to Gb3Cer (d18:1, C24:0) were not accompanied by ions indicative of Gb3Cer (d18:1, C24:1) and Gb3Cer (d18:1, C22:0) (Fig. 6B, left panel), which were clearly detectable as minor ions in the mass spectrum of total cell neutral GSLs (Fig. 2B, left panel). Furthermore, ions at m/z 1186.83, which correspond to Gb3Cer (d18:1, C26:0), were found considerably enriched in the DRM fraction 2 (Fig. 6B, left panel) but were almost undetectable in the

upper Gb3Cer positive band of total cells (Fig. 2B, left panel). The m/z values of 1146.67 acquired from the lower immunopositive Gb3Cer band gave evidence for Gb3Cer (d18:1, C16:0) as the only Gb3Cer variant with short-chain fatty acid in DRM fraction 2 (Fig. 6B, right panel) as observed for the neutral GSL fraction of total EA.hy 926 cells (Fig. 2B, right panel). A synopsis of the relative m/z intensities attributable to the different Gb3Cer lipofoms is presented in Table 1.

Immunofluorescence microscopic detection of Gb3Cer, caveolin-1, and flotillin-2

The subcellular localization of Gb3Cer and DRM-associated marker proteins caveolin-1 and flotillin-2 in HBMECs and EA.hy 926 cells was evaluated after Triton X-100 permeabilization (Fig. 7). Antibody detection of Gb3Cer revealed a broad distribution in both endothelial cell lines, whereby HBMECs exhibited a more regular and homogenous distribution of Gb3Cer clusters compared to EA.hy 926 cells. The caveolae and lipid raft marker proteins, caveolin-1 and flotillin-2, respectively, appeared distinguishable from each other in differently clustered structures and obviously did not localize in identical fluorescence spots in HBMECs (Fig. 7A) or EA.hy 926 cells (Fig. 7B), indicating their subdistribution to different types of microdomains. Furthermore, flotillin-2 and Gb3Cer seemed to reside in more punctate structures than caveolin-1 in both types of endothelial cells. Higher-resolution imaging using confocal microscopy is required to address the question of colocalization of Gb3Cer with the two lipid raft marker proteins. However, it is noteworthy that flotillin-2 exhibits a subcellular distribution different from that previously observed in kidney epithelium (69) and oligodendroglial cells (70).

To address the issue of surface localization of Gb3Cer, we produced immunofluorescence micrographs of non-permeabilized HBMECs and EA.hy 926 cells (supplementary Fig. II). HBMECs seem to harbor considerable amounts of Gb3Cer on the cell surface, whereas EA.hy 926 cells obviously express less abundant Gb3Cer molecules in

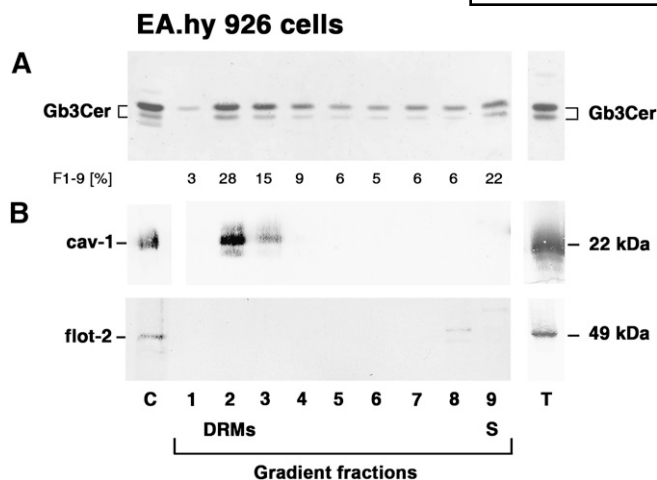


Fig. 5. Detection of Gb3Cer (A) and caveolin-1 and flotillin-2 (B) in sucrose gradient fractions of EA.hy 926 cells. Gradient fractions were numbered from top (= fraction 1) to bottom (= fraction 8); fraction 9 was obtained by solubilization of the sediment (see supplementary Fig. 1). A: TLC overlay assay. Lipid extracts were separated by TLC, and Gb3Cer was immunodetected with anti-Gb3Cer antibody. Control (C): 2 μ g of neutral GSLs from human erythrocytes; GSL amounts of the gradient fractions 1-9 (F1-9) correspond to 5×10^5 cells, and those of total cells (T) are equivalent to 2.5×10^5 cells. The relative amounts of Gb3Cer within the gradient fractions (F1-9) were determined densitometrically and are given as percentages in the figure; different Gb3Cer lipofoms (upper and lower bands) of total cells and DRM fraction 2 are listed as percentages in Table 2. B: Western blots. Protein preparations were separated by SDS-PAGE and transferred onto nitrocellulose membranes. Caveolin-1 and flotillin-2 were detected with anti-caveolin-1 (upper panel) and anti-flotillin-2 antibody (lower panel). Control (C): 10 μ g of human heart lysate and 20 μ g of HeLa cell lysate for caveolin-1 and flotillin-2 immunodetection, respectively; protein amounts of the sucrose gradient fractions 1-9 and total cells (T) correspond to 1×10^6 cells, respectively. Vertical white lines indicate areas of noncontiguous lanes assembled. DRM, detergent-resistant membrane; EA.hy 926 cells, HUVEC descendant cell line; Gb3Cer, globotriaosylceramide; Gb4Cer, globotetraosylceramide; GSL, glycosphingolipid; S, sediment fraction.

the plasma membrane. Owing to their localization to the inner leaflet of the plasma membrane bilayer, caveolin-1 and flotillin-2 were undetectable in nonpermeabilized cells (data not shown).

Cholesterol and protein content of sucrose density gradient fractions after M β CD-treatment

A series of control experiments was performed with HBMECs and EA.hy 926 cells employing different culture conditions and various concentrations of M β CD in serum-free medium for cholesterol depletion of the plasma membranes. The experiments, aimed at the determination of M β CD-caused effects on the cholesterol, GSL, and lipid raft marker protein composition of DRMs, were performed under serum-free conditions with 10 mM of M β CD (supplementary Fig. III).

The lipid extracts and protein preparations of sucrose density gradient fractions from HBMECs and EA.hy 926 cells were examined as described above after cholesterol depletion of the cell cultures with 10 mM M β CD. The most

obvious effect observed was the considerably diminished cholesterol content in DRM fraction 2 and adjacent fractions 1 and 3 of HBMECs and EA.hy 296 cells, respectively (Fig. 8A) compared with untreated cells (see Fig. 3A). The average reduction of cholesterol in DRM fraction 2 and adjacent fractions 1 and 3 of HBMECs after M β CD-treatment was 55%, leaving 45% in intact DRMs. The simultaneous increase in the other gradient fractions, particularly in fractions 7 to 9, suggested a low release of approximately 25% of cholesterol, most likely into the environmental culture medium. In contrast, the average cholesterol content of DRM fraction 2 and fractions 1 and 3 of EA.hy 926 cells was reduced to 96%, indicating an almost complete M β CD-mediated destruction of cholesterol-containing microdomains, which harbored only 4% of the original cholesterol before M β CD incubation (Fig. 8A). The slight concomitant increase in fraction 7 and the almost entire loss of cholesterol in the sediment fraction 9 pointed to a high release of approximately 87% of cholesterol, most probably into the cell culture medium as calculated from the total remaining cholesterol content of the gradient fractions. Importantly, the primary cholesterol content was 1.8- and 1.4-times higher in DRM fraction 2 and adjacent fraction 3 of EA.hy 926 cells, respectively, compared with HBMECs (see Fig. 3A), whereas after M β CD exposure, the remaining cholesterol in the corresponding fractions of HBMECs was found to be 6 and 7.5 times higher, respectively (Fig. 8A), indicating a greater loss of cholesterol in EA.hy 296 cells. These findings clearly evidenced a pronounced refractiveness and thus a more stable molecular assembly of microdomains in HBMECs toward M β CD-mediated cholesterol depletion compared to EA.hy 926 cells.

Determinations of the protein concentrations (Fig. 8B) revealed for both endothelial cell lines an overall diminishment in the DRM fraction 2 and contiguous fraction 3 and the intermediate gradient fractions 4 to 6, similar amounts in fraction 7, and reduction of the protein content in the bottom fraction 8 and the sediment fraction 9 after M β CD-exposure (see Fig. 3B). The lower protein quantity of the latter two fractions was more pronounced for EA.hy 926 cells. The total recovery rate of proteins in the gradient fractions after M β CD-treatment was higher for HBMECs, and the calculated environmental release of membrane proteins of DRM fraction 2 and flanking fraction 3 amounted on average of both fractions to 34% for HBMECs and 52% for EA.hy 926 cells. Thus, the higher segregation rate of cholesterol that was calculated for EA.hy 926 cells coincided with a concomitant enhanced loss of cholesterol-associated membrane proteins, giving further evidence for the existence of microdomains with higher resistance to M β CD treatment in HBMECs.

Distribution of Gb3Cer and Gb4Cer to sucrose gradient fractions of HBMECs after M β CD-mediated cholesterol depletion

To elucidate the influence of cholesterol depletion on the distribution of Gb3Cer and Gb4Cer as well as caveolin-1 and flotillin-2 to sucrose gradient fractions of HBMECs, TLC overlay assays and Western blots were performed

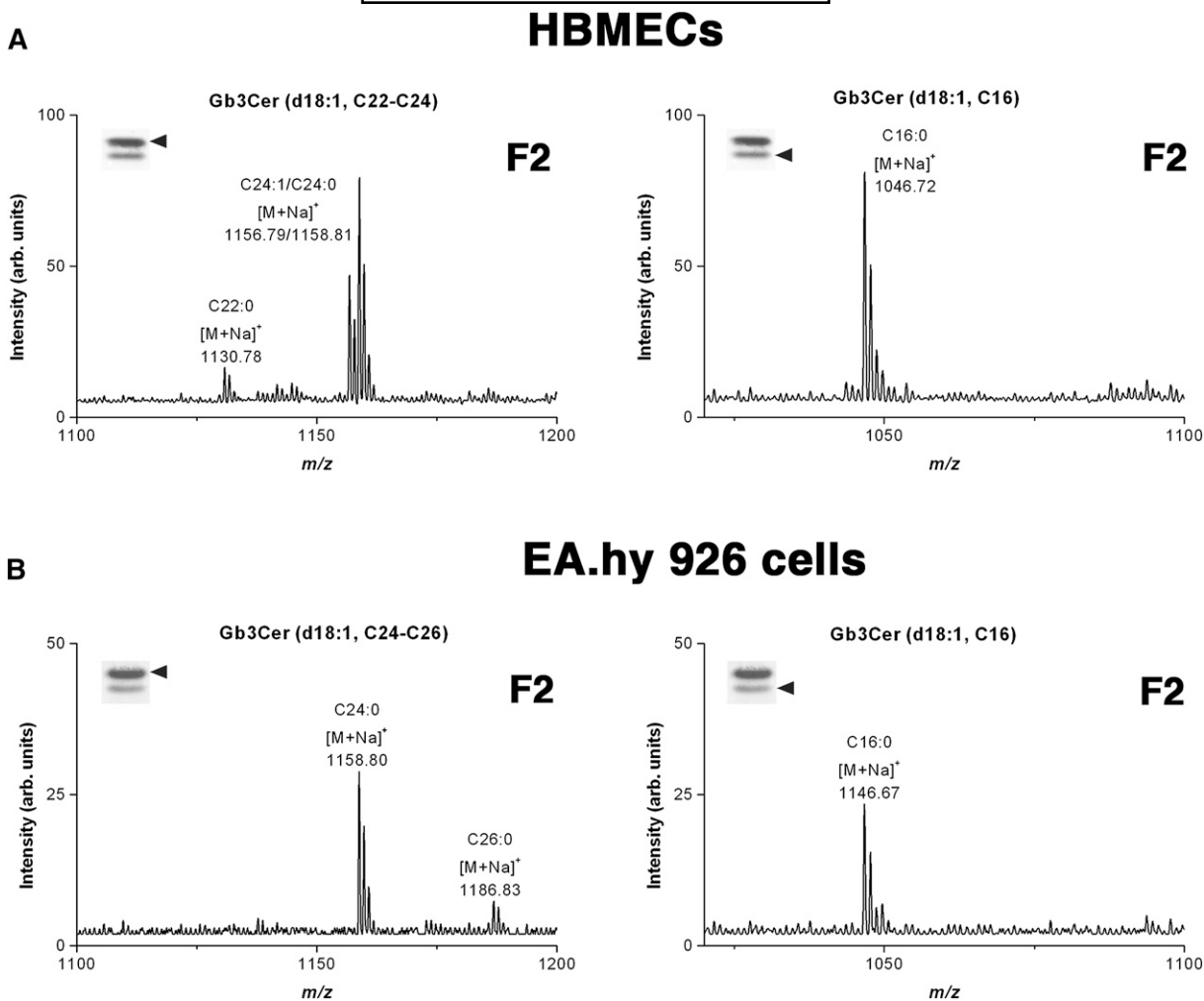


Fig. 6. TLC-IR-MALDI-o-TOF mass spectra obtained from antibody-detected Gb3Cer species in DRM fraction 2 of HBMECs (A) and EA.hy 926 cells (B). The overlay assays were performed with TLC-separated lipid extracts corresponding to 3×10^5 cells. The in situ analyzed Gb3Cer positive upper bands (left panels) and lower bands (right panels) are marked with arrowheads in the insets. Mass spectra were acquired in the positive ion mode; Gb3Cer species were detected as singly charged monosodium [M+Na]⁺ ions. Relative ion intensities of detected Gb3Cer variants are listed in Table 1. The sucrose density gradient fractions 2 (F2) enriched in DRMs are shown for HBMECs and EA.hy 926 cells in Fig. 4A and Fig. 5A, respectively. DRM, detergent-resistant membrane; EA.hy 926 cells, HUVEC descendant cell line; Gb3Cer, globotriaosylceramide; HBMEC, human brain microvascular endothelial cell; IR-MALDI, infrared matrix-assisted laser desorption/ionization; o-TOF, orthogonal time-of-flight.

after exposure to 10 mM M β CD and gradient fractionation (Fig. 9). Cholesterol depletion resulted in a pattern of Gb3Cer bands residing with 53%, 22%, and 3% in DRM fraction 2 and adjacent gradient fractions 3 and 1, respectively (Fig. 9A, upper panel). Thus, 78% of Gb3Cer floated in the DRM fractions. The remaining 12% accounted for soluble Gb3Cer in the nonDRM fractions 4 to 8, and 10% were detected in the sediment fraction, indicating slight relative reduction of Gb3Cer in the DRM fractions compared with untreated HBMECs (see Fig. 4A, upper panel). Quantitation of summed fractions 1 to 3 in relation to the control immunostains on the same TLC plates revealed 94% maintenance of DRM-associated Gb3Cer after cholesterol depletion. The ratios of Gb3Cer species with long- (upper band) to short-chain (lower band) fatty acids upon M β CD exposure were almost identical to those determined in DRM fraction 2 and total cells of untreated HBMECs (Table 2).

Gb4Cer distributed with 51%, 20%, and 1% to DRM fraction 2 and contiguous fractions 3 and 1, respectively (Fig. 9A, lower panel). Thus, 72% of Gb4Cer floated in the DRM fractions. The residual 16% constituted soluble Gb4Cer in the nonDRM fractions 4 to 8, and 12% were present in the sediment fraction, indicating a slight relative increase of Gb4Cer in the sediment fraction but, in general, a similar pattern compared with untreated HBMECs (see Fig. 4A, lower panel). A maintenance level of 60% after cholesterol depletion was calculated for summed DRM fractions 1 to 3 in relation to the control immunostains on the same TLC plates. Interestingly, whereas the ratios of long- (upper band) and short-chain (lower band) fatty acid harboring Gb4Cer variants remained largely stable in total cells, a considerable rise of Gb4Cer (d18:1, C22-C24) from 57% to 73% could be determined in DRM fraction 2 after M β CD-mediated cholesterol depletion (Table 2). As a conclusion, treatment of HBMECs with

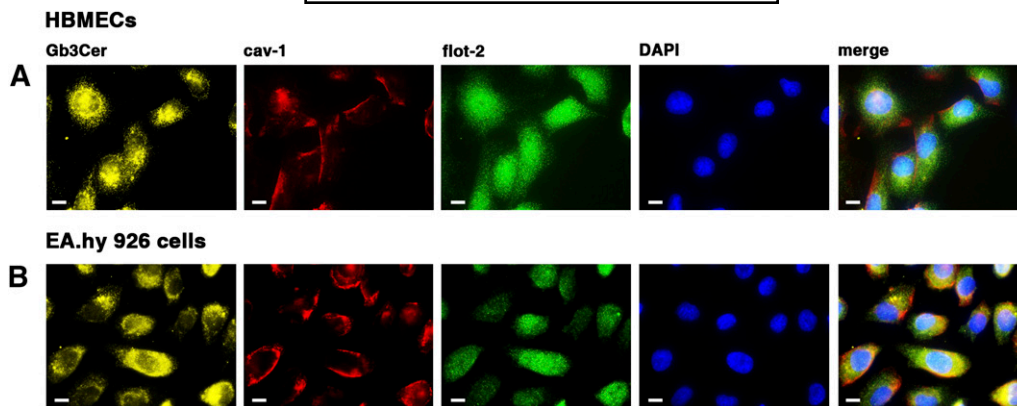


Fig. 7. Indirect immunofluorescence microscopic detection of Gb3Cer, caveolin-1, and flotillin-2 in permeabilized HBMECs (A) and EA.hy 926 cells (B). Endothelial cells were grown to subconfluence in 8-well chamber slides and permeabilized with 0.3% Triton X-100. Detection was performed with rat 38.13 anti-Gb3Cer, rabbit anti-caveolin-1, and mouse B-6 anti-flotillin-2 antibodies, followed by incubation with Alexa Fluor[®] 546, Alexa Fluor[®] 488, and Cy5[®] labeled secondary antibodies, respectively. Cell nuclei were stained with DAPI. Bars: 10 μ m. DAPI, 4'-6-diamidino-2-phenylindol; EA.hy 926 cells, HUVEC descendant cell line; Gb3Cer, globotriaosylceramide; HBMEC, human brain microvascular endothelial cell.

M β CD demonstrated high maintenance levels for both Gb3Cer and Gb4Cer, distinguishable by significantly higher content of Gb3Cer in the DRM fractions pointing to a particularly stable association of Gb3Cer with remaining cholesterol in the DRM fractions.

The Western blot analysis of caveolae and lipid raft marker proteins revealed moderate appearance of caveolin-1 in DRM fraction 2, accompanied by enhanced content in the nonDRM fractions 7 and 8 as a consequence of M β CD treatment (Fig. 9B, upper panel) compared with untreated cells (see Fig. 4B, upper panel). In addition, a strong rise of flotillin-2 was observed in DRM fraction 2, and mildly increased levels were found in gradient fraction 3 and sediment fraction 9 after cholesterol elimination (Fig. 9B, lower panel) as the most impressive change compared with HBMECs, which were not exposed to M β CD (see Fig. 4B, lower panel). Together the data suggested a partial destruction of lipid rafts caused by cholesterol depletion, indicated by decline of GSLs in the DRM fraction along with rising soluble caveolin-1 in nonDRM fractions, as well as an obvious dynamic replenishment of DRM fraction 2 by flotillin-2 and its exceptionally firm association with the remaining cholesterol and GSLs.

Distribution of Gb3Cer to sucrose gradient fractions of EA.hy 926 cells after M β CD-mediated cholesterol depletion

The same approach (i.e., exposure to 10 mM M β CD and gradient fractionation, followed by TLC overlay detection of Gb3Cer and Western blot investigation of lipid raft marker proteins) was applied to EA.hy 926 cells (Fig. 10). As deduced from the TLC overlay assay, only faint immunoreactive bands were observed due to very low quantities of Gb3Cer detectable in the gradient fractions (Fig. 10A). However, Gb3Cer was found to distribute with 34%, 16%, and 3% to DRM fraction 2 and adjacent fractions 3 and 1, respectively. Thus, 53% of Gb3Cer floated in the DRM

fractions. The remaining 30% accounted for soluble Gb3Cer in the nonDRM fractions 4 to 8, and 17% were attributable to the sediment fraction after cholesterol removal, evidencing similar relative distribution of Gb3Cer in the DRM fractions compared with EA.hy 926 cells without cholesterol depletion (see Fig. 5A). Importantly, quantitation of summed fractions 1 to 3 in relation to the control immunostains on the same TLC plates revealed an extremely low maintenance of DRM associated Gb3Cer of only 9% after cholesterol depletion. The ratios of Gb3Cer species with long- (upper band) to short-chain (lower band) fatty acids upon M β CD exposure were similar to those obtained from DRM fraction 2 and total cells of untreated EA.hy 926 cells (Table 2). In conclusion, incubation with M β CD resulted in a tremendous reduction of DRMs accompanied by an almost entire loss of Gb3Cer in the corresponding gradient fractions, suggesting an extremely labile GSL-cholesterol assembly in microdomains of EA.hy 926 cells.

Despite the approximately 90% reduction in DRMs, the caveolae marker caveolin-1 was still clearly detectable in DRM fraction 2 along with a considerable increase of soluble caveolin-1 in the bottom fraction 8 after M β CD treatment (Fig. 10B, upper panel). Flotillin-2 was again undetectable in DRMs (Fig. 10B, lower panels) as observed in gradient fractions obtained from cells without M β CD exposure (Fig. 5B, lower panel). Together the data evidenced an almost complete destruction of lipid rafts caused by cholesterol depletion, along with a 90% decline of Gb3Cer in the DRM fraction with rising soluble caveolin-1, which suggested a rather labile lipid assembly in microdomains of EA.hy 926 cells.

GSL expression of EA.hy 926 cells after medium change

Because culturing cells in different types of media (e.g., DMEM:F12 or RPMI 1640) may alter their biochemical

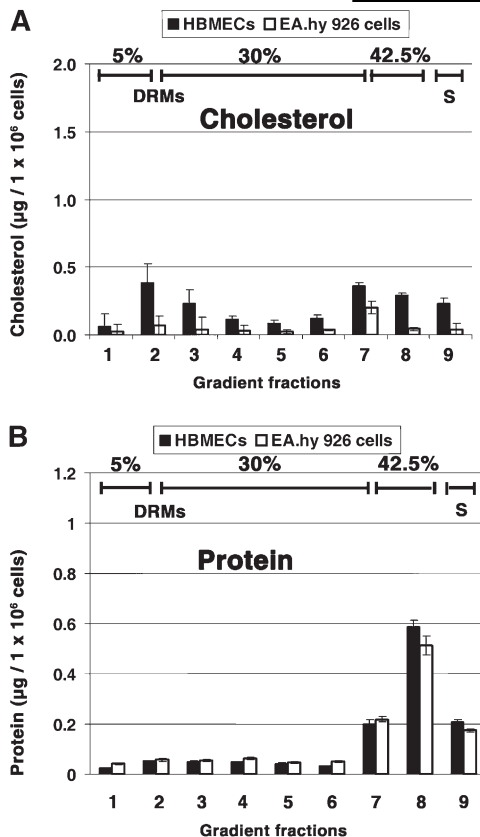


Fig. 8. Cholesterol (A) and protein (B) content in sucrose density gradient fractions of HBMECs (black bars) and EA.hy 926 cells (white bars) after treatment with 10 mM M β CD. Gradient fractions were numbered from top (= fraction 1) to bottom (= fraction 8); fraction 9 was obtained by solubilization of the sediment. Lipid extracts were separated by TLC, and cholesterol was quantified by densitometric scanning. Stained proteins were quantified colorimetrically by extinction measurement in microtiter plates. Results represent the means and standard deviations of 3-fold determination and are expressed as micrograms per 1×10^6 cells. DRM, detergent-resistant membrane; EA.hy 926 cells, HUVEC descendant cell line; HBMEC, human brain microvascular endothelial cell; M β CD, methyl- β -cyclodextrin; S, sediment fraction.

nature (71), we cultivated EA.hy 926 cells in the same medium as HBMECs (RPMI 1640 medium) and investigated the possible influence of the cell culture medium on GSL expression, particularly on the inability of Gb4Cer biosynthesis. The medium shift from DMEM:F12 to RPMI 1640 did not cause any changes related to EA.hy 926 cell morphology, growth behavior, adhesiveness, or confluence degree as demonstrated for cells grown in original DMEM:F12 and after 10 passages in RPMI 1640 medium (supplementary Fig. IV). Furthermore, triple experiments of EA.hy 926 cells propagated in the two different media revealed the same GSL profile concerning Gb3Cer abundancy and lack of Gb4Cer (see supplementary Fig. V). The Gb3Cer profiles of EA.hy 926 cells propagated in original DMEM:F12 and after switching to RPMI 1640 were comparable (supplementary Fig. V-A, lanes c and d). Moreover, the lack of Gb4Cer expression was observed in both media (supplementary Fig. V-B, lanes c and d), indicating this failure as an intrinsic feature of EA.hy 926 cells as previously reported (52).

HBMECs + 10 mM M β CD

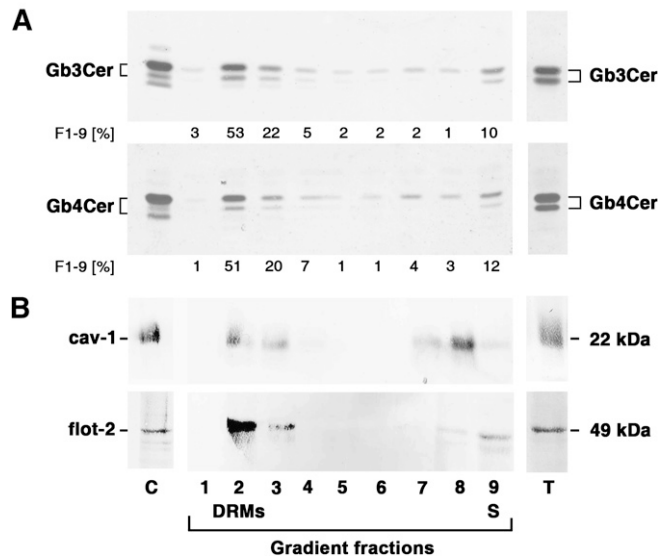


Fig. 9. Detection of Gb3Cer and Gb4Cer (A) and caveolin-1 and flotillin-2 (B) in sucrose gradient fractions of HBMECs after treatment with 10 mM M β CD. Gradient fractions were numbered from top (= fraction 1) to bottom (= fraction 8); fraction 9 was obtained by solubilization of the sediment (see supplementary Fig. I). A: TLC overlay assays. Lipid extracts were separated by TLC and Gb3Cer and Gb4Cer were immunodetected with anti-Gb3Cer antibody (upper panel) and anti-Gb4Cer antibody (lower panel), respectively. Control (C): 2 μ g and 0.2 μ g of neutral GSLs from human erythrocytes for anti-Gb3Cer and anti-Gb4Cer immunostain, respectively; GSL amounts of the gradient fractions 1-9 (F1-9) correspond to 5×10^5 cells, and those of total cells (T) are equivalent to 2.5×10^5 cells. The relative amounts of Gb3Cer and Gb4Cer within the gradient fractions (F1-9) were determined densitometrically and are given as percentages in the figure; different Gb3Cer and Gb4Cer lipofoms (upper and lower bands) of total cells and DRM fraction 2 are listed as percentages in Table 2. B: Western blots. Protein preparations were separated by SDS-PAGE and transferred onto nitrocellulose membranes. Caveolin-1 and flotillin-2 were detected with anti-caveolin-1 antibody (upper panel) and anti-flotillin-2 antibody (lower panel). Control (C): 10 μ g of human heart lysate and 20 μ g of HeLa cell lysate for caveolin-1 and flotillin-2 immunodetection, respectively; protein amounts of the sucrose gradient fractions 1-9 and total cells (T) correspond to 1×10^6 cells, respectively. Vertical white lines indicate areas of non-contiguous lanes assembled. DRM, detergent-resistant membrane; Gb3Cer, globotriaosylceramide; Gb4Cer, globotetraosylceramide; GSL, glycosphingolipid; HBMEC, human brain microvascular endothelial cell; M β CD, methyl- β -cyclodextrin; S, sediment fraction.

Distribution of Gb3Cer to sucrose gradient fractions of EA.hy 926 cells after medium change

TLC immunodetection of Gb3Cer in lipid extracts and Western blots of caveolin-1 and flotillin-2 in protein preparations of the gradient fractions after medium shift of EA.hy 926 cells are shown in Fig. 11. Gb3Cer was prevalent in DRM fraction 2 and also present in accompanying fractions 1 and 3, composing 52% compared with the remaining gradient fractions with higher sucrose density (Fig. 11A). This result was comparable with data from EA.hy 926 cells grown in original DMEM:F12, where 46% of Gb3Cer distributed to DRM fraction 2 and the two adjacent fractions (see Fig. 5A).

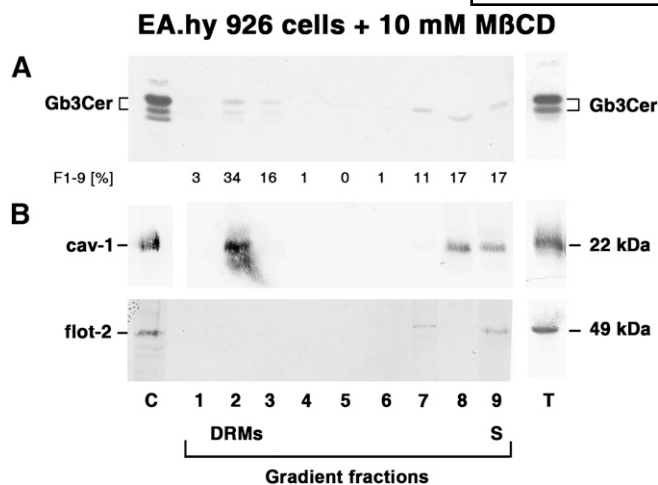


Fig. 10. Detection of Gb3Cer (A) and caveolin-1 and flotillin-2 (B) in sucrose gradient fractions of EA.hy 926 cells after treatment with 10 mM MβCD. Gradient fractions were numbered from top (= fraction 1) to bottom (= fraction 8); fraction 9 was obtained by solubilization of the sediment (see supplementary Fig. 1). A: TLC overlay assays. Lipid extracts were separated by TLC, and Gb3Cer was immunodetected with anti-Gb3Cer antibody. Control (C): 2 μg of neutral GSLs from human erythrocytes; GSL amounts of the gradient fractions 1-9 (F1-9) correspond to 5×10^5 cells, and those of total cells (T) are equivalent to 2.5×10^5 cells. The relative amounts of Gb3Cer within the gradient fractions (F1-9) were determined densitometrically and are given as percentages in the figure; different Gb3Cer lipofoms (upper and lower bands) of total cells and DRM fraction 2 are listed as percentages in Table 2. B: Western blots. Protein preparations were separated by SDS-PAGE and transferred onto nitrocellulose membranes. Caveolin-1 and flotillin-2 were detected with anti-caveolin-1 antibody (upper panel) and anti-flotillin-2 antibody (lower panel). Control (C): 10 μg of human heart lysate and 20 μg of HeLa cell lysate for caveolin-1 and flotillin-2 immunodetection, respectively; protein amounts of the sucrose gradient fractions 1-9 and total cells (T) correspond to 1×10^6 cells, respectively. Vertical white lines indicate areas of noncontiguous lanes assembled. DRM, detergent-resistant membrane; EA.hy 926 cells, HUVEC descendant cell line; Gb3Cer, globotriaosylceramide; GSL, glycosphingolipid; MβCD, methyl-β-cyclodextrin; S, sediment fraction.

The strong appearance of caveolin-1 in the Western blots of DRM fraction 2 and adjacent fraction 3 (Fig. 11B, upper panel) was consistent with former results of EA.hy 926 cells grown in DMEM:F12 (see Fig. 5B, upper panel). Flotillin-2 was detectable only in trace quantities in DRM fraction 2 and fraction 8 (Fig. 11B, lower panel), comparable to the Western blot obtained from EA.hy 926 cells before the medium shift (see Fig. 5B, lower panel). In conclusion, the medium switch did not significantly change the expression of either Gb3Cer or the two lipid raft marker proteins.

Distribution of Gb3Cer to sucrose gradient fractions of EA.hy 926 cells after medium change and MβCD-mediated cholesterol depletion

TLC overlay detection of Gb3Cer and Western blot determination of lipid raft marker proteins of EA.hy 926 cells after medium shift and MβCD-mediated cholesterol depletion is shown in Fig. 12. Only trace quantities of

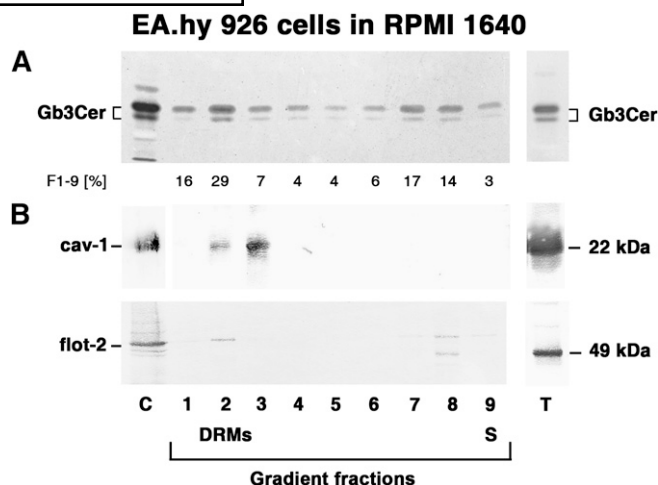


Fig. 11. Detection of Gb3Cer (A) and caveolin-1 and flotillin-2 (B) in sucrose gradient fractions of EA.hy 926 cells after medium switch to RPMI 1640. Gradient fractions were numbered from top (= fraction 1) to bottom (= fraction 8); fraction 9 was obtained by solubilization of the sediment (see supplementary Fig. 1). A: TLC overlay assays of lipid extracts from gradient fractions 1-9 (F1-9) and of total cells (T) were performed as described in Fig. 5A. B: Western blots of SDS-PAGE separated protein preparations from gradient fractions 1-9 and total cells were performed as described in Fig. 5B. Vertical white lines indicate areas of noncontiguous lanes assembled. DRM, detergent-resistant membrane; EA.hy 926 cells, HUVEC descendant cell line; Gb3Cer, globotriaosylceramide; S, sediment fraction.

Gb3Cer were detectable in all of the gradient fractions as deduced from the TLC overlay assay (Fig. 12A). The overall reduction in distribution of Gb3Cer to DRM fractions was the same as observed for EA.hy 926 cells cultivated in original DMEM:F12 followed by cholesterol depletion (see Fig. 10A), which indicated same lability toward MβCD treatment after the medium switch.

Caveolin-1 dominated in DRM fraction 2 and the gradient fractions with high sucrose density (Fig. 12B, upper panel), while flotillin-2 remained largely undetectable with the exception of the sediment fraction 9 (Fig. 12B, lower panel), which was quite similar to the findings in the original DMEM:F12 after cholesterol depletion (see Fig. 10). Together the data confirmed a less stable lipid assembly in microdomains of EA.hy 926 cells, which was only marginally influenced by the cell culture medium.

DISCUSSION

Since it was first described as a simple barrier between extra and intracellular compartments, different plasma membrane structural and composition models have been proposed (2). Over the last decade, several works have provided evidence that the plasma membrane is indeed more mosaic than fluid (32). It is now widely accepted that the lateral organization of cellular membranes is formed by the clustering of specific lipids, such as cholesterol and GSLs, into highly condensed microdomains, and that the formation and disassembly of lipid raft domains is a dynamic process (1).

**EA.hy 926 cells in RPMI 1640
 + 10 mM MβCD**

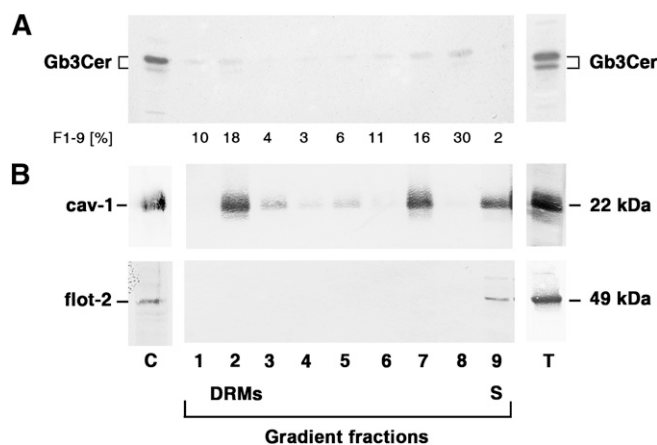


Fig. 12. Detection of Gb3Cer (A) and caveolin-1 and flotillin-2 (B) in sucrose gradient fractions of EA.hy 926 cells after medium switch to RPMI 1640 and treatment with 10 mM MβCD. Gradient fractions were numbered from top (= fraction 1) to bottom (= fraction 8); fraction 9 was obtained by solubilization of the sediment (see supplementary Fig. 1). A: TLC overlay assays of lipid extracts from gradient fractions 1-9 (F1-9) and of total cells (T) were performed as described in Fig. 10A. B: Western blots of SDS-PAGE separated protein preparations from gradient fractions 1 to 9 and total cells were performed as described in Fig. 10B. Vertical white lines indicate areas of noncontiguous lanes assembled. DRM, detergent-resistant membrane; EA.hy 926 cells, HUVEC descendant cell line; Gb3Cer, globotriaosylceramide; MβCD, methyl-β-cyclodextrin; S, sediment fraction.

The tight packaging of cholesterol, GSLs, and phospholipids confers to lipid rafts their resistance to solubilization by nonionic detergents in the cold. Detergent resistance reflects a stronger lateral interaction between membrane components, which allows their separation and isolation as DRMs from the rest of the plasma membrane using sucrose-density gradients (65, 72). We found that Stx receptors preferentially localized to the liquid-ordered phases of DRM fractions of HBMECs and EA.hy 926 cells, where they colocalized with prevalent flotillin-2 and caveolin-1, respectively. Note that the ratio of insoluble versus soluble Gb3Cer was higher in HBMECs, whereas there was a considerably lower Gb3Cer association with DRMs and a concomitant increase of soluble Gb3Cer in nonDRM fractions of EA.hy 926 cells. We previously described that EA.hy 926 cells exhibited a higher sensitivity to Stx1 and a higher mortality rate in vitro compared with HBMECs (52). A very recent study of our group on the direct comparison of both types of endothelial cells using quantitative apoptosis/necrosis assay (73) revealed different susceptibilities to Stx1 and Stx2: EA.hy 926 cells were slightly, but significantly (~10 times), more sensitive to Stx1, whereas HBMECs were strikingly (≥1,000 times) more susceptible to Stx2. These findings were quite surprising because Stx1 and Stx2 are known to exhibit identical receptor binding specificity, and both EA.hy 926 cells and HBMECs express the high-affinity receptor Gb3Cer in relevant quantities (52), suggesting the existence of yet-to-be delineated Stx

type-specific mechanisms of endothelial cell injury beyond inhibition of protein biosynthesis (73). Furthermore, one would expect a higher susceptibility of HBMECs toward Stx due to higher content of DRM-associated Stx receptors as shown in this study, but this is only the case for Stx2 (73). Thus, with the current knowledge regarding Stx-receptor content and plasma membrane localization as well as lipid raft association, we do not know the reasons for the observed differential cytotoxic action of Stx1 and Stx2. Further investigations are required using confocal laser microscopy, which has been employed successfully for subcellular routing of Stx and localization of flotillin by Sandvig and coworkers (74, 75).


However, there seems to be no question that Gb3Cer within DRMs, an index of GSL-cholesterol-enriched lipid rafts, is required for in vitro cytotoxicity (47, 49, 76, 77) and may define glomeruli-restricted pathology (78), whereas randomly distributed Gb3Cer in the nonordered liquid state may have a protective effect. The most plausible reason for this is that the internalized Stx B-subunit-Gb3Cer complex derived from soluble Gb3Cer is trafficked to the lysosomes where the toxin is degraded, resulting in survival of the cells (47). It is well accepted that the presence of Gb3Cer within DRMs is central for the ensuing transport of the Gb3Cer/Stx agglomerate via endosomes and the trans-Golgi network to the endoplasmic reticulum. In addition, the translocation of the A-subunit from the endoplasmic reticulum into the cytosol depends largely on Gb3Cer assembly in DRMs (49). However, the molecular arrangement of soluble Gb3Cer and Gb4Cer in non-DRM fractions remains obscure and raises the question of whether the GSLs distribute as single molecules or whether a so-far unknown cholesterol-free association with soluble proteins might exist, especially in the liquid-disordered phase of the gradient bottom fraction containing the highest sucrose concentration.

A relevant specific enrichment of certain lipofoms (i.e., GSL variants with long- and short-chain fatty acids) in DRMs compared with total cell extracts could not be detected, although a subtle change in favor of Gb3Cer with C24 fatty acid was arguable in DRM fraction 2 of HBMECs as deduced from TLC overlay assays, accompanied by a small relative increase of monounsaturated C24:1 fatty detectable by in situ TLC-IR-MALDI-o-TOF-MS. Lingwood et al. proposed that the heterogeneity in fatty acid composition of GSLs may mediate aglycone (ceramide) regulation of GSL membrane receptor function by a differential interaction with cholesterol and other membrane components that may be differentially organized within plasma membrane lipid domains (79, 80). These concepts have been illustrated in model membrane studies, particularly in relation to Gb3Cer-Stx-interaction. Importantly, mixtures containing Gb3Cer with C18 fatty acid were not recognized by Stx1, but the addition of the Gb3Cer variant with C24:1 fatty acid resulted in the generation of presentation and binding platforms for Stx1, whereas Stx2 bound Gb3Cer species largely irrespective of fatty acid chain length (81). Those studies indicated that fatty acid-mediated fluidity within simple GSL and cholesterol-containing

DRMs can selectively regulate GSL carbohydrate ligand binding. We found the classical TLC-separated Gb3Cer doublets in HBMECs and EA.hy 296 cells consisting of Gb3Cer (d18:1, C24:1/C24:0) in the faster and Gb3Cer (d18:1, C16:0) in the slower moving band in both cell lines but no Gb3Cer lipofoms with C18 and C20 fatty acids (52). Because the latter have been reported to fail in binding to Stx1 in Gb3Cer-cholesterol vesicles (81), this suggests involvement of at least Gb3Cer (d18:1, C24:1/C24:0), but the participation of Gb3Cer (d18:1, C16:0) in the recognition process of Stx1 and Stx2 in HBMECs and EA.hy 926 cells is unknown. We aim therefore to unravel in the near future the functional role of these DRM-associated Gb3Cer species to explain the differential cytotoxic actions of Stx1 and Stx2 toward the different types of endothelial cells (73).

As Stx cytotoxicity and retrograde trafficking have been shown for HeLa and glomerular microvascular endothelial cell cultures to depend on Gb3Cer presence within DRMs (47, 82), whereas randomly distributed Gb3Cer in the plasma membrane was found to mediate binding and subsequent traffic to lysosomes for Stx degradation in HeLa and bovine epithelial cells (47, 76), we investigated the destabilization of endothelial DRMs employing cholesterol-sequestering M β CD. Cholesterol, as a dynamic “glue” holding lipid rafts together, was only incompletely removed from the plasma membrane of HBMECs by M β CD treatment, giving evidence for highly refractive microdomains in the liquid-ordered membrane phase. The remaining and rather high cholesterol content of 45% in the DRMs correlated with only marginally diminished Gb3Cer retaining the same C24 to C16 fatty acid ratio compared with DRMs of untreated cells. In contrast to Gb3Cer, a disproportionately high loss of Gb4Cer accompanied by a simultaneous substantial loss of Gb4Cer with C16 fatty acid indicated less stable raft-insertion of Gb4Cer with the short-chain fatty acid as the most plausible explanation for high extraction efficacy. In contrast to HBMECs, exposure to M β CD resulted in almost completely abolished cholesterol content of 9% in macrovascular EA.hy 926 cells, in accordance with exceptionally low Gb3Cer content of 10%. We do not know the membrane constituents that might confer structural stability to lipid rafts of HBMECs or why microdomains of HBMECs and EA.hy 926 cells are distinct in terms of sensitivity toward cholesterol depletion. However, it is tempting to speculate that, for example, the observed replenishment of DRM fractions by flotillin-2 may support the stability of lipid rafts through cholesterol removal, pointing to a dynamic process of membrane reconstitution by auxiliary membrane proteins. Moreover, besides unique GSL requirements for functionally intact lipid rafts (26, 83), it is unclear whether GSL-GSL interaction may contribute to lipid raft solidity and thus to refractiveness through cholesterol depletion. In this context, it is noteworthy that an association of Gb3Cer with other GSLs or functionally different pools of Gb3Cer may be involved in lipid raft dynamics (48, 49). However, it should be mentioned that these studies, including the impressive investigations on Stx-mediated induction of

tubular membrane invaginations which hint to a perplexing diversity of endocytic routes (84), have been performed with nonendothelial cells, and generalizations for endothelial cells are therefore limited.

Thus, despite the hypothetical functional role of GSL association with lipid rafts in endothelial cells, our study provides some useful information and the basis for future investigations to clarify the involvement of raft-associated GSLs in uptake and trafficking of Stx to intracellular targets. Our study may contribute to a deeper understanding of Stx-mediated endothelial cell injury. 

REFERENCES

1. Lingwood, D., and K. Simons. 2010. Lipid rafts as a membrane-organizing principle. *Science*. **327**: 46–50.
2. Pike, L. J. 2003. Lipid rafts: bringing order to chaos. *J. Lipid Res.* **44**: 655–667.
3. Bauer, M., and L. Pelkmans. 2006. A new paradigm for membrane-organizing and -shaping scaffolds. *FEBS Lett.* **580**: 5559–5564.
4. Yu, C., M. Alterman, and R. T. Dobrowsky. 2005. Ceramide displaces cholesterol from lipid rafts and decreases the association of the cholesterol binding protein caveolin-1. *J. Lipid Res.* **46**: 1678–1691.
5. Rothberg, K. G., J. E. Heuser, W. C. Donzell, Y-S. Ying, J. R. Glenney, and R. G. Anderson. 1992. Caveolin, a protein component of caveolae membrane coats. *Cell*. **68**: 673–682.
6. Glebov, O. O., N. A. Bright, and B. J. Nichols. 2006. Flotillin-1 defines a clathrin-independent endocytic pathway in mammalian cells. *Nat. Cell Biol.* **8**: 46–54.
7. Fielding, C. J., and P. E. Fielding. 1997. Intracellular cholesterol transport. *J. Lipid Res.* **38**: 1503–1521.
8. Gargalovic, P., and L. Dory. 2003. Caveolins and macrophage lipid metabolism. *J. Lipid Res.* **44**: 11–21.
9. Parton, R. G., and A. A. Richards. 2003. Lipid rafts and caveolae as portals for endocytosis: new insights and common mechanisms. *Traffic*. **4**: 724–738.
10. Zheng, Y. Z., and L. J. Foster. 2009. Contributions of quantitative proteomics to understanding membrane microdomains. *J. Lipid Res.* **50**: 1976–1985.
11. Sprenger, R. R., D. Speijer, J. W. Back, C. G. de Koster, H. Pannekoek, and A. J. G. Horrevoets. 2004. Comparative proteomics of human endothelial cell caveolae and rafts using two-dimensional gel electrophoresis and mass spectrometry. *Electrophoresis*. **25**: 156–172.
12. Karsan, A., J. Blonder, J. Law, E. Yaquian, D. A. Lucas, T. P. Conrads, and T. Veenstra. 2005. Proteomic analysis of lipid microdomains from lipopolysaccharide-activated human endothelial cells. *J. Proteome Res.* **4**: 349–357.
13. Gupta, G., and A. Surolia. 2010. Glycosphingolipids in microdomain formation and their spatial organization. *FEBS Lett.* **584**: 1634–1641.
14. Levery, S. B. 2005. Glycosphingolipid structural analysis and glycosphingolipidomics. *Methods Enzymol.* **405**: 300–369.
15. Müthing, J., and U. Distler. 2010. Advances on the compositional analysis of glycosphingolipids combining thin-layer chromatography with mass spectrometry. *Mass Spectrom. Rev.* **29**: 425–479.
16. Lopez, P. H., and R. L. Schnaar. 2009. Gangliosides in cell recognition and membrane protein regulation. *Curr. Opin. Struct. Biol.* **19**: 549–557.
17. Miller-Podraza, H., L. Johansson, P. Johansson, T. Larsson, M. Matrosovich, and K-A. Karlsson. 2000. A strain of human influenza A virus binds to extended but not short gangliosides as assayed by thin-layer chromatography overlay. *Glycobiology*. **10**: 975–982.
18. Campanero-Rhodes, M. A., A. Smith, W. Chai, S. Sonnino, L. Mauri, R. A. Childs, Y. Zhang, H. Ewers, A. Helenius, A. Imberty, et al. 2007. N-Glycolyl GM1 ganglioside as a receptor for simian virus 40. *J. Virol.* **81**: 12846–12858.
19. Karlsson, K-A. 1989. Animal glycosphingolipids as membrane attachment sites for bacteria. *Annu. Rev. Biochem.* **58**: 309–350.
20. Miller-Podraza, H., P. Johansson, J. Ångström, T. Larsson, M. Longard, and K-A. Karlsson. 2004. Studies on gangliosides with affinity for *Helicobacter pylori*: binding to natural and chemically modified structures. *Glycobiology*. **14**: 205–217.

21. Lingwood, C. A., H. Law, S. Richardson, M. Petric, J. L. Brunton, S. De Grandis, and M. Karmali. 1987. Glycolipid binding of purified and recombinant *Escherichia coli* produced verotoxin in vitro. *J. Biol. Chem.* **262**: 8834–8839.
22. Müthing, J., C. H. Schweppe, H. Karch, and A. W. Friedrich. 2009. Shiga toxins, glycosphingolipid diversity, and endothelial cell injury. *Thromb. Haemost.* **101**: 252–264.
23. Merrill, A. H., Jr., M. D. Wang, M. Park, and M. C. Sullards. 2007. (Glyco)sphingolipidology: an amazing challenge and opportunity for systems biology. *Trends Biochem. Sci.* **32**: 457–468.
24. Merrill, A. H., Jr., T. H. Stokes, A. Momin, H. Park, B. J. Portz, S. Kelly, E. Wang, M. C. Sullards, and M. D. Wang. 2009. Sphingolipidomics: a valuable tool for understanding the roles of sphingolipids in biology and disease. *J. Lipid Res.* **50**: S97–S102.
25. Li, Y., P. Thapa, D. Hawke, Y. Kondo, K. Furukawa, K. Furukawa, F.-F. Hsu, D. Adlercreutz, J. Weadge, M. M. Palcic, et al. 2009. Immunologic glycosphingolipidomics and NKT cell development in mouse thymus. *J. Proteome Res.* **8**: 2740–2751.
26. Raa, H., S. Grimmer, D. Schwudke, J. Bergan, S. Wälchli, T. Skotland, A. Shevchenko, and K. Sandvig. 2009. Glycosphingolipid requirements for endosome-to-Golgi transport of Shiga toxin. *Traffic*. **10**: 868–882.
27. Li, Y., S. Teneberg, P. Thapa, A. Bendelac, S. B. Levery, and D. Zhou. 2008. Sensitive detection of isoglobo and globo series tetraglycosylceramides in human thymus by ion trap mass spectrometry. *Glycobiology*. **18**: 158–165.
28. Li, Y., D. Zhou, C. Xia, P. G. Wang, and S. B. Levery. 2008. Sensitive quantitation of isoglobotriaosylceramide in the presence of isobaric components using electrospray ionization-ion trap mass spectrometry. *Glycobiology*. **18**: 166–176.
29. Shaner, R. L., J. C. Allegood, H. Park, E. Wang, S. Kelly, C. A. Haynes, M. C. Sullards, and A. H. Merrill, Jr. 2009. Quantitative analysis of sphingolipids for lipidomics using triple quadrupole and quadrupole linear ion trap mass spectrometers. *J. Lipid Res.* **50**: 1692–1707.
30. Li, Y., E. Arigi, H. Eichert, and S. B. Levery. 2010. Mass spectrometry of fluorocarbon-labeled glycosphingolipids. *J. Mass Spectrom.* **45**: 504–519.
31. Fuchs, B., R. Süss, and J. Schiller. 2010. An update of MALDI-TOF mass spectrometry in lipid research. *Prog. Lipid Res.* **49**: 450–475.
32. Pike, L. J. 2009. The challenge of lipid rafts. *J. Lipid Res.* **50**: S323–S328.
33. Gillard, B. K., M. A. Jones, and D. M. Marcus. 1987. Glycosphingolipids of human umbilical vein endothelial cells and smooth muscle cells. *Arch. Biochem. Biophys.* **256**: 435–445.
34. Müthing, J., S. Duvar, D. Heitmann, F. G. Hanisch, U. Neumann, G. Lochnit, R. Geyer, and J. Peter-Katalinić. 1999. Isolation and structural characterization of glycosphingolipids of in vitro propagated human umbilical vein endothelial cells. *Glycobiology*. **9**: 459–468.
35. Okuda, T., S.-I. Nakakita, and K.-I. Nakayama. 2010. Structural characterization and dynamics of globotetraosylceramide in vascular endothelial cells under TNF- α stimulation. *Glycoconj. J.* **27**: 287–296.
36. Bielaszewska, M., and H. Karch. 2005. Consequences of enterohaemorrhagic *Escherichia coli* infection for the vascular endothelium. *Thromb. Haemost.* **94**: 312–318.
37. Karch, H., P. I. Tarr, and M. Bielaszewska. 2005. Enterohaemorrhagic *Escherichia coli* in human medicine. *Int. J. Med. Microbiol.* **295**: 405–418.
38. Tarr, P. I., C. A. Gordon, and W. L. Chandler. 2005. Shiga toxin-producing *Escherichia coli* and haemolytic uraemic syndrome. *Lancet*. **365**: 1073–1086.
39. Hurley, B. P., C. M. Thorpe, and D. W. Acheson. 2001. Shiga toxin translocation across intestinal epithelial cells is enhanced by neutrophil transmigration. *Infect. Immun.* **69**: 6148–6155.
40. Brigotti, M., D. Carnicelli, E. Ravanelli, S. Barbieri, F. Ricci, A. Bontadini, A. E. Tozzi, G. Scavia, A. Caprioli, and P. L. Tazzari. 2008. Interactions between Shiga toxins and human polymorphonuclear leukocytes. *J. Leukoc. Biol.* **84**: 1019–1027.
41. Brigotti, M., P. L. Tazzari, E. Ravanelli, D. Carnicelli, S. Barbieri, L. Rocchi, V. Arfilli, G. Scavia, F. Ricci, A. Bontadini, et al. 2010. Endothelial damage induced by Shiga toxins delivered by neutrophils during transmigration. *J. Leukoc. Biol.* **88**: 201–210.
42. Sandvig, K., Ø. Garred, K. Prydz, J. V. Kozlov, S. H. Hansen, and B. van Deurs. 1992. Retrograde transport of endocytosed Shiga toxin to the endoplasmic reticulum. *Nature*. **358**: 510–512.
43. Sandvig, K. 2001. Shiga toxins. *Toxicol.* **39**: 1629–1635.
44. Sandvig, K., M. L. Torgersen, N. Engedal, T. Skotland, and T.-G. Iversen. 2010. Protein toxins from plants and bacteria: probes for intracellular transport and tools in medicine. *FEBS Lett.* **584**: 2626–2634.
45. Kovbasnjuk, O., M. Edidin, and M. Donowitz. 2001. Role of lipid rafts in Shiga toxin I interaction with the apical surface of Caco-2 cells. *J. Cell Sci.* **114**: 4025–4031.
46. Hanashima, T., M. Miyake, K. Yahiro, Y. Iwamaru, A. Ando, N. Morinaga, and M. Noda. 2008. Effect of Gb3 in lipid rafts in resistance to Shiga-like toxin of mutant Vero cells. *Microb. Pathog.* **45**: 124–133.
47. Falguières, T., F. Mallard, C. Baron, D. Hanau, C. Lingwood, B. Gould, J. Salamero, and L. Johannes. 2001. Targeting of Shiga toxin B-subunit to retrograde transport route in association with detergent-resistant membranes. *Mol. Biol. Cell.* **12**: 2453–2468.
48. Falguières, T., W. Römer, M. Amessou, C. Afonso, C. Wolf, J. C. Tabet, C. Lamaze, and L. Johannes. 2006. Functionally different pools of Shiga toxin receptor, globotriaosyl ceramide, in HeLa cells. *FEBS J.* **273**: 5205–5218.
49. Smith, D. C., D. J. Sillescu, T. Falguières, R. M. Jarvis, L. Johannes, J. M. Lord, F. M. Platt, and L. M. Roberts. 2006. The association of Shiga-like toxin with detergent-resistant membranes is modulated by glucosylceramide and is an essential requirement in the endoplasmic reticulum for a cytotoxic effect. *Mol. Biol. Cell.* **17**: 1375–1387.
50. Fujinaga, Y., A. A. Wolf, C. Rodighiero, H. Wheeler, B. Tsai, L. Allen, M. G. Jobling, T. Rapoport, R. K. Holmes, and W. I. Lencer. 2003. Gangliosides that associate with lipid rafts mediate transport of cholera and related toxins from the plasma membrane to endoplasmic reticulum. *Mol. Biol. Cell.* **14**: 4783–4793.
51. Lencer, W. I., and D. Saslowsky. 2005. Raft trafficking of AB₅ subunit bacterial toxins. *Biochim. Biophys. Acta.* **1746**: 314–321.
52. Schweppe, C. H., M. Bielaszewska, G. Pohlentz, A. W. Friedrich, H. Büntemeyer, M. A. Schmidt, K. S. Kim, J. Peter-Katalinić, H. Karch, and J. Müthing. 2008. Glycosphingolipids in vascular endothelial cells: relationship of heterogeneity in Gb3Cer/CD77 receptor expression with differential Shiga toxin 1 cytotoxicity. *Glycoconj. J.* **25**: 291–304.
53. Stins, M. F., F. Gilles, and K. S. Kim. 1997. Selective expression of adhesion molecules on human brain microvascular endothelial cells. *J. Neuroimmunol.* **76**: 81–90.
54. Edgell, C. J. S., C. C. McDonald, and J. B. Graham. 1983. Permanent cell line expressing human factor VIII-related antigen established by hybridization. *Proc. Natl. Acad. Sci. USA.* **80**: 3734–3737.
55. Ledeen, R. W., and R. K. Yu. 1982. Gangliosides: structure, isolation, and analysis. *Methods Enzymol.* **83**: 139–191.
56. Müthing, J., U. Maurer, K. Šoštarić, U. Neumann, H. Brandt, S. Duvar, J. Peter-Katalinić, and S. Weber-Schürholz. 1994. Different distributions of glycosphingolipids in mouse and rabbit skeletal muscle demonstrated by biochemical and immunohistological analyses. *J. Biochem.* **115**: 248–256.
57. Meisen, I., A. W. Friedrich, H. Karch, U. Witting, J. Peter-Katalinić, and J. Müthing. 2005. Application of combined high-performance thin-layer chromatography immunostaining and nano-electrospray ionization quadrupole time-of-flight tandem mass spectrometry to the structural characterization of high- and low-affinity binding ligands of Shiga toxin 1. *Rapid Commun. Mass Spectrom.* **19**: 3659–3665.
58. Schweppe, C. H., P. Hoffmann, J.-R. Nofer, G. Pohlentz, M. Mormann, H. Karch, A. W. Friedrich, and J. Müthing. 2010. Neutral glycosphingolipids in human blood: a precise mass spectrometry analysis with special reference to lipoprotein-associated Shiga toxin receptors. *J. Lipid Res.* **51**: 2282–2294.
59. Distler, U., J. Souady, M. Hülsewig, I. Drmić-Hofman, J. Haier, A. W. Friedrich, H. Karch, N. Senninger, K. Dreisewerd, S. Berkenkamp, et al. 2009. Shiga toxin receptor Gb3Cer/CD77: tumor association and promising therapeutic target in pancreas and colon cancer. *PLoS ONE*. **4**: e6813.
60. Hoffmann, P., M. Hülsewig, S. Duvar, H. Ziehr, M. Mormann, J. Peter-Katalinić, A. W. Friedrich, H. Karch, and J. Müthing. 2010. On the structural diversity of Shiga toxin glycosphingolipid receptors in lymphoid and myeloid cells determined by nano-electrospray ionization tandem mass spectrometry. *Rapid Commun. Mass Spectrom.* **24**: 2295–2304.
61. Chester, M. A. 1998. IUPAC-IUB Joint Commission on Biochemical Nomenclature (IUB). Nomenclature of glycolipids. Recommendations 1997. *Eur. J. Biochem.* **257**: 293–298.

62. Müthing, J. 1998. TLC in structure and recognition studies of glycosphingolipids. *In* Methods in Molecular Biology. E. F. Hounsell, editor. Humana Press Inc., Totawa, NJ. 183–195.
63. Goswami, S. K., and C. F. Frey. 1970. Manganous chloride spray reagent for cholesterol and bile acids on thin-layer chromatograms. *J. Chromatogr. A*. **53**: 389–390.
64. Distler, U., M. Hülsewig, J. Souady, K. Dreisewerd, J. Haier, N. Senninger, A. W. Friedrich, H. Karch, F. Hillenkamp, S. Berkenkamp, et al. 2008. Matching IR-MALDI-o-TOF mass spectrometry with the TLC overlay binding assay and its clinical application for tracing tumor-associated glycosphingolipids in hepatocellular and pancreatic cancer. *Anal. Chem.* **80**: 1835–1846.
65. Brown, D. A., and J. K. Rose. 1992. Sorting of GPI-anchored proteins to glycolipid-enriched membrane subdomains during transport to the apical cell surface. *Cell*. **68**: 533–544.
66. Lowry, O. H., N. J. Rosebrough, A. L. Farr, and R. J. Randall. 1951. Protein measurement with the Folin phenol reagent. *J. Biol. Chem.* **193**: 265–275.
67. Laemmli, U. K. 1970. Cleavage of structural proteins during the assembly of the head of bacteriophage T4. *Nature*. **227**: 680–685.
68. Dreisewerd, K., J. Müthing, A. Rohlfing, I. Meisen, Ž. Vukelić, J. Peter-Katalinić, F. Hillenkamp, and S. Berkenkamp. 2005. Analysis of gangliosides directly from thin-layer chromatography plates by infrared matrix-assisted laser desorption/ionization orthogonal time-of-flight mass spectrometry with a glycerol matrix. *Anal. Chem.* **77**: 4098–4107.
69. Roitbak, T., Z. Surviladze, R. Tikkanen, and A. Wandinger-Ness. 2005. A polycystin multiprotein complex constitutes a cholesterol-containing signalling microdomain in human kidney epithelia. *Biochem. J.* **392**: 29–38.
70. Trajkovic, K., C. Hsu, S. Chiantia, L. Rajendran, D. Wenzel, F. Wieland, P. Schwille, B. Brügger, and M. Simons. 2008. Ceramide triggers budding of exosome vesicles into multivesicular endosomes. *Science*. **319**: 1244–1247.
71. Cohly, H., J. Stephens, A. Markhov, M. Angel, W. Campbell, K. Ndebele, and J. Jenkins. 2001. Cell culture conditions affect LPS inducibility of the inflammatory mediators in J774A.1 murine macrophages. *Immunol. Invest.* **30**: 1–15.
72. Lingwood, D., and K. Simons. 2007. Detergent resistance as a tool in membrane research. *Nat. Protoc.* **2**: 2159–2165.
73. Bauwens, A., M. Bielaszewska, B. Kemper, P. Langehanenberg, G. von Bally, R. Reichelt, D. Mulac, H-U. Humpff, A. W. Friedrich, K. S. Kim, et al. Differential cytotoxic actions of Shiga toxin 1 and Shiga toxin 2 on microvascular and macrovascular endothelial cells. *Thromb. Haemost.* Epub ahead of print. December 6, 2010; doi: 10.1160/TH10-02-0140.
74. Sandvig, K., J. Bergan, A-B. Dyve, T. Skotland, and M. L. Torgersen. 2010. Endocytosis and retrograde transport of Shiga toxin. *Toxicol.* **56**: 1181–1185.
75. Pust, S., A. B. Dyve, M. L. Torgersen, B. van Deurs, and K. Sandvig. 2010. Interplay between toxin transport and flotillin localization. *PLoS ONE*. **5**: e8844.
76. Hoey, D. E. E., L. Sharp, C. Currie, C. A. Lingwood, D. L. Gally, and D. G. E. Smith. 2003. Verotoxin 1 binding to intestinal crypt epithelial cells results in localization to lysosomes and abrogation of toxicity. *Cell. Microbiol.* **5**: 85–97.
77. Tam, P., R. Mahfoud, A. Nutikka, A. A. Khine, B. Binnington, P. Paroutis, and C. Lingwood. 2008. Differential intracellular transport and binding of verotoxin 1 and verotoxin 2 to globotriaosylceramide-containing lipid assemblies. *J. Cell. Physiol.* **216**: 750–763.
78. Khan, F., F. Proulx, and C. A. Lingwood. 2009. Detergent-resistant globotriaosyl ceramide may define verotoxin/glomeruli-restricted hemolytic uremic syndrome pathology. *Kidney Int.* **75**: 1209–1216.
79. Lingwood, C. A., A. Manis, R. Mahfoud, F. Khan, B. Binnington, and M. Mylvaganam. 2010. New aspects of the regulation of glycosphingolipid receptor function. *Chem. Phys. Lipids*. **163**: 27–35.
80. Lingwood, C. A., B. Binnington, A. Manis, and D. R. Branch. 2010. Globotriaosyl ceramide receptor function - where membrane structure and pathology intersect. *FEBS Lett.* **584**: 1879–1886.
81. Mahfoud, R., A. Manis, and C. A. Lingwood. 2009. Fatty acid-dependent globotriaosyl ceramide receptor function in detergent resistant model membranes. *J. Lipid Res.* **50**: 1744–1755.
82. Warnier, M., W. Römer, J. Geelen, J. Lesieur, M. Amessou, L. van den Heuvel, L. Monnens, and L. Johannes. 2006. Trafficking of Shiga toxin/Shiga-like toxin-1 in human glomerular microvascular endothelial cells and human mesangial cells. *Kidney Int.* **70**: 2085–2091.
83. Cheng, Z-J., R. D. Singh, D. K. Sharma, E. L. Holicky, K. Hanada, D. L. Marks, and R. E. Pagano. 2006. Distinct mechanisms of clathrin-independent endocytosis have unique sphingolipid requirements. *Mol. Biol. Cell.* **17**: 3197–3210.
84. Römer, W., L. Berland, V. Chambon, K. Gaus, B. Windschiegl, D. Tenza, M. R. Aly, V. Fraisier, J-C. Florent, D. Perrais, et al. 2007. Shiga toxin induces tubular membrane invaginations for its uptake into cells. *Nature*. **450**: 670–675.